



www.maajournal.com

Mediterranean Archaeology and Archaeometry
Vol. 21, No 3, (2021), pp. 89-122
Open Access. Online & Print.



DOI: 10.5281/zenodo.5598239

CHEMICAL COMPOSITION AND MICROSTRUCTURE ANALYSIS OF PLASTER AND PIGMENTS RETRIEVED FROM A DECORATED HOUSE WALL AT SELEUCID TELL IZTABBA (NUSA-SCYTHOPOLIS, BETH SHE'AN, ISRAEL)

Dana Ashkenazi^{*1}, Romi Shnabel², Achim Lichtenberger³ and Oren Tal²

¹*School of Mechanical Engineering, Tel Aviv University, Ramat Aviv 6997801, Israel*

²*Department of Archaeology and Ancient Near Eastern Cultures, Tel Aviv University, Ramat Aviv, 6997801, Israel*

³*Westfälische Wilhelms-Universität Münster, Institut für Klassische Archäologie und Christliche Archäologie/Archäologisches Museum, Domplatz 20-22, D-48143 Münster, Germany*

Received: 19/10/2021

Accepted: 01/11/2021

*Corresponding author: Dana Ashkenazi (danaa@tauex.tau.ac.il)

ABSTRACT

Fragments of wall paintings retrieved from Hellenistic Tell Iztabba (Nusa-Scythopolis), an archaeological site located in the area of the Beth She'an Valley (Israel), are the subject of this study. This research aims to characterize the plaster and color pigments of wall paintings retrieved from the site in order to gain new information concerning their nature, their origin and the technologies that were used to paint the walls of a Hellenistic settlement in the Near East. For that purpose, visual testing inspection, XRF, SEM-EDS, and XRD analyses were applied combined with archaeological and geographical data. As the site was founded in the 160s BCE and destructed in 108/07 BCE, the material analyzed is not only stratigraphically well-secured but also well-dated to the mid-second century BCE. The walls of the dwellings under discussion were painted by the fresco method and the white-hued plaster was made of calcium carbonate matrix with embedded aggregates. The red and yellow paints were identified as red and yellow ochre pigments, respectively. The brown paint was a mixture of red ochre, yellow ochre, magnetite mineral and carbon black-based pigments. The black paint was identified as carbon black-based pigment. The pigments were mixed with fine plaster powder. The plaster and pigments were most likely regionally (if not locally) produced and supplied and provide us with information about the technical knowledge of the inhabitants of the Seleucid settlement.

KEYWORDS: Nusa (Scythopolis), Hellenistic, Plaster, Fresco, Pigments, Secco.

1. INTRODUCTION

Tell Iẓṭabba is the main settlement of Seleucid Nysa-Scythopolis (Beth Sh'e'an). The site is located in the Beth She'an Valley (Fig. 1). Earlier excavations at the site were undertaken sporadically in the 1950s (by N. Zori), in 1977 (by V. Tzaferis) and from 1991 to 1994 (by R. Bar-Nathan and G. Mazor) (see Ebeling *et al.*, 2020, pp. 177–178). Since 2019, the site has been investigated by a joint German-Israeli team aiming at a systematic understanding of the settlement history and

economics of the Seleucid site as it is of major interest for the study of the Hellenistic period in the region. Our German-Israeli Tell Iẓṭabba Excavation Project undertakes a comprehensive archaeological investigation of the site based on geophysical prospections (Lichtenberger *et al.*, 2020) (Fig. 2) and archaeological excavations (Ebeling *et al.*, 2020; 2021) (Fig. 3) in order to gain new insights into the nature of the Seleucid settlement there and thus expand our knowledge of Seleucid engagement in the region.

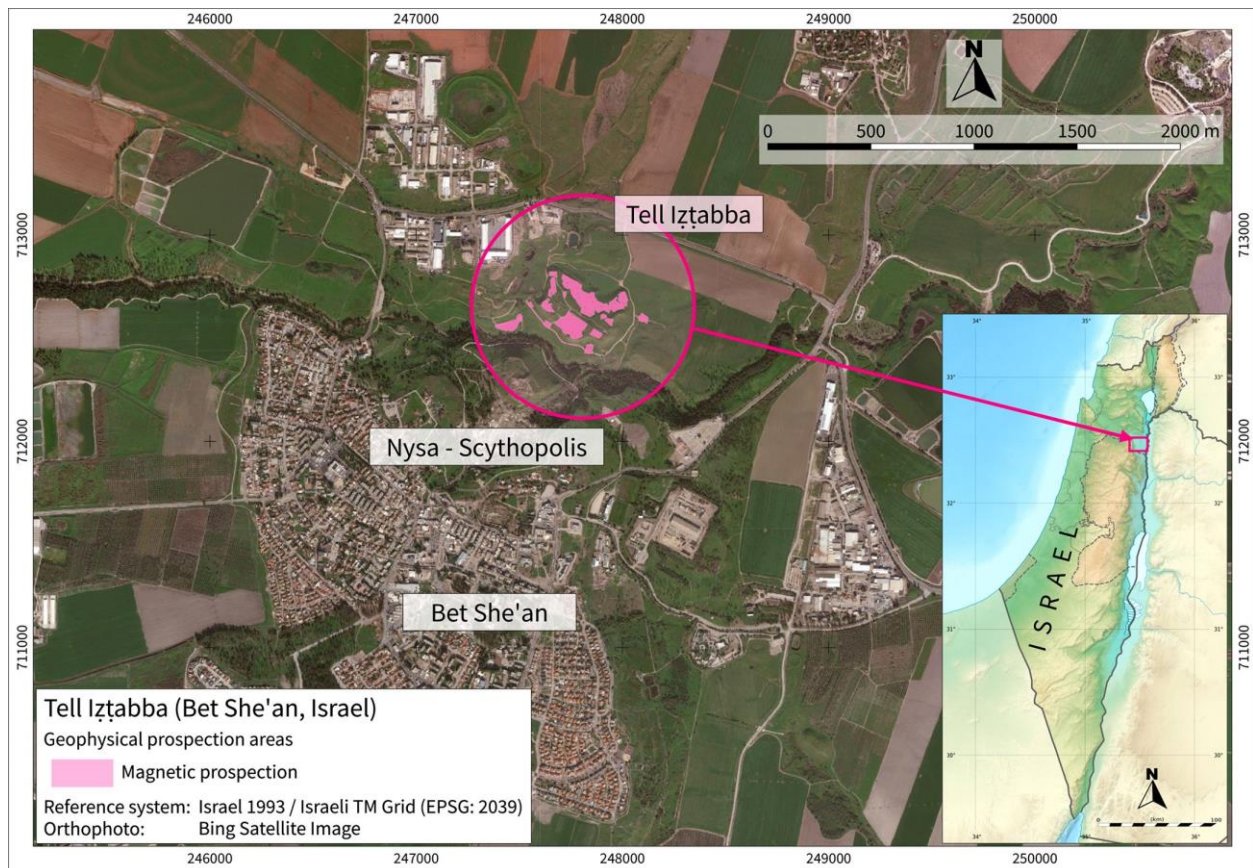


Figure 1. Map showing the location of Tell Iẓṭabba (East), in the Beth She'an Valley, Israel (©German-Israeli Tell Iẓṭabba Excavation Project).

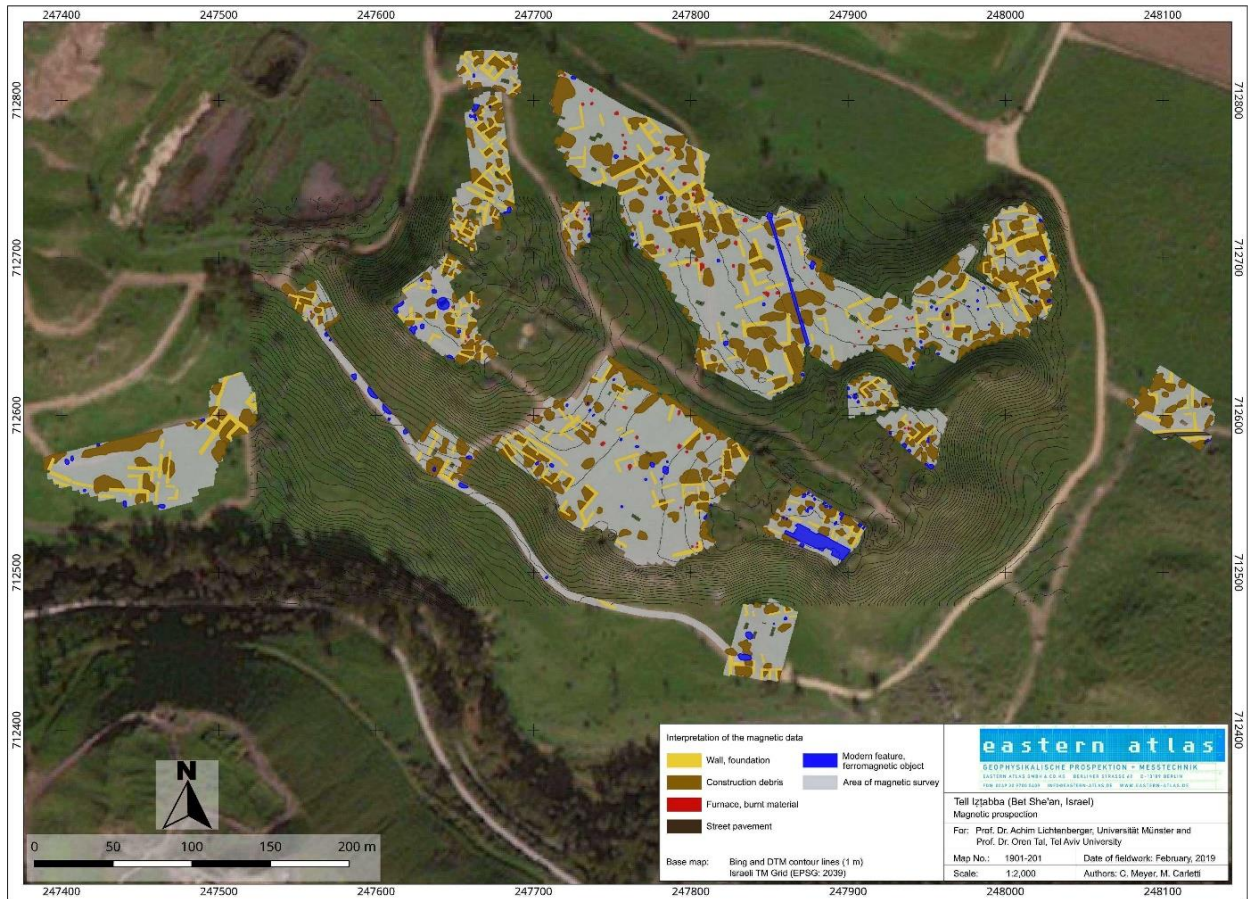


Figure 2. Aerial photograph of Tell İztabba (East) with interpretation of magnetic data (©German-Israeli Tell İztabba Excavation Project).

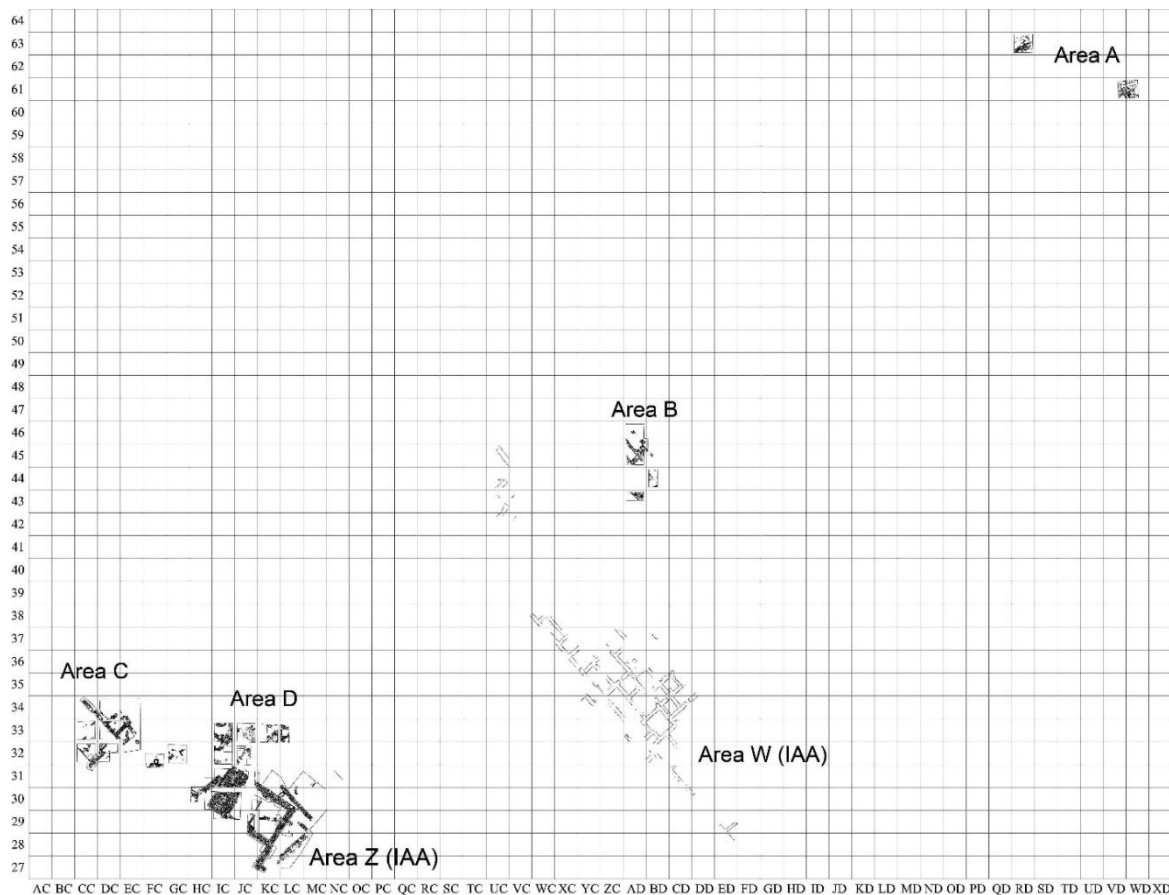


Figure 3. Plan of Tell Iztabba (East) with excavated areas of the Israel Antiquities Authority (W and Z) and the German-Israeli Tell Iztabba Excavation Project (A–D) (©German-Israeli Tell Iztabba Excavation Project).

Nysa-Scythopolis belonged to a group of Graeco-Roman cities that were supported by the Hellenistic dynasties – first the Ptolemies and later the Seleucids – and these cities later formed a group named Decapolis (Tal, 2011; Lichtenberger, 2020). One of the major formation phases of these cities was in the time of Antiochos IV, who founded several towns in the region in the 160s BCE (Lichtenberger, 2008). These urban centers were surrounded by less urbanized entities, such as the Jewish state of the Hasmoneans or the Nabataeans, and came into conflict with them. The Seleucid settlement of Nysa-Scythopolis was destroyed by the Hasmonean John Hyrcanus I in 108/07 BCE, providing us with a fixed terminus ante quem for the settlement (Josephus Ant. 13.280; cf. Finkielsztein 1999). Since it was only founded about half a century earlier, all the material culture of the city stems from a short period of time.

Nysa-Scythopolis was one of the sites founded by Antiochos IV and it is generally assumed that Greek settlers populated the newly founded city. This can also be inferred from the material culture of the Hellenistic settlement that was excavated by the Israel Antiquities Authority in the 1990s and now in the ongoing German-Israeli project. The pottery and espe-

cially the amphorae suggest Greek consumption habits of a community that was well connected with the Mediterranean region (Mazor *et al.*, 2018). Glass (Jackson-Tal *et al.*, 2021), plaster and stucco remains, as well as metal objects indicate that the community oriented towards the Hellenistic lifestyle but agricultural production and use of mudbrick architecture also indicate an embeddedness in local knowledge cultures (Orendi *et al.*, 2021).

This research focuses on plaster and stucco remains retrieved from one of the walls (Wall 307) of a domestic structure we excavated in Area C (cf. Ebeling *et al.*, 2020, pp. 184–187) (Fig. 4). The plaster and stucco remains were not unearthed in situ on the walls; rather, they came from the floor level, Locus 324 and the fill below it, Locus 326, after having fallen off the walls due to the structure's destruction as well as post depositional processes (Fig. 5). They were found when we excavated the foundation courses of Wall 307. The analyzed fragments together with many others that came from our Areas C and B, as well as the previous Israel Antiquities Authority excavations (Mazor *et al.*, 2018, p. 3) can be assigned to the “first Pompeian style”/“Masonry Style”, typical of the Hellenistic period and the Hellenistic Levant (Laidlaw, 1985; Ling,

1991, pp. 12–99). This style which imitates regular masonry in plastered relief, was analyzed from a stylistic perspective at Levantine Hellenistic sites such as Jebel Khalid, Syria (Jackson, 2016), or in Israel at Beth Yerah/Philoteria (Tal and Reshef, 2017, pp. 28–30), Ashkelon (Birney, 2017) and Tel Anafa, where the painted plaster remains were analyzed chemically as well (Kidd, 2018); it is also attested in later Herodian/Early Roman (and Roman) sites in Judaea (Foerster, 1995, pp. 51–80; see also Rozenberg, 2008 and esp. 298–310 for a survey of sites in the region). This research aims to characterize the plaster and color

pigments of wall paintings retrieved from the Hellenistic (Seleucid) period dwellings of Tell İztabba by using an interdisciplinary approach, combining chemical composition and microstructure analysis results with archaeological and geographical data, in order to gain novel information concerning the nature of the pigments, including whether they were locally produced or imported, and the technologies that were used to paint the walls. Our study as formulated below comes to increase our knowledge concerning the use of plaster in Hellenistic Palestine and about the technological knowledge of a newly founded Hellenistic colony in the Near East.

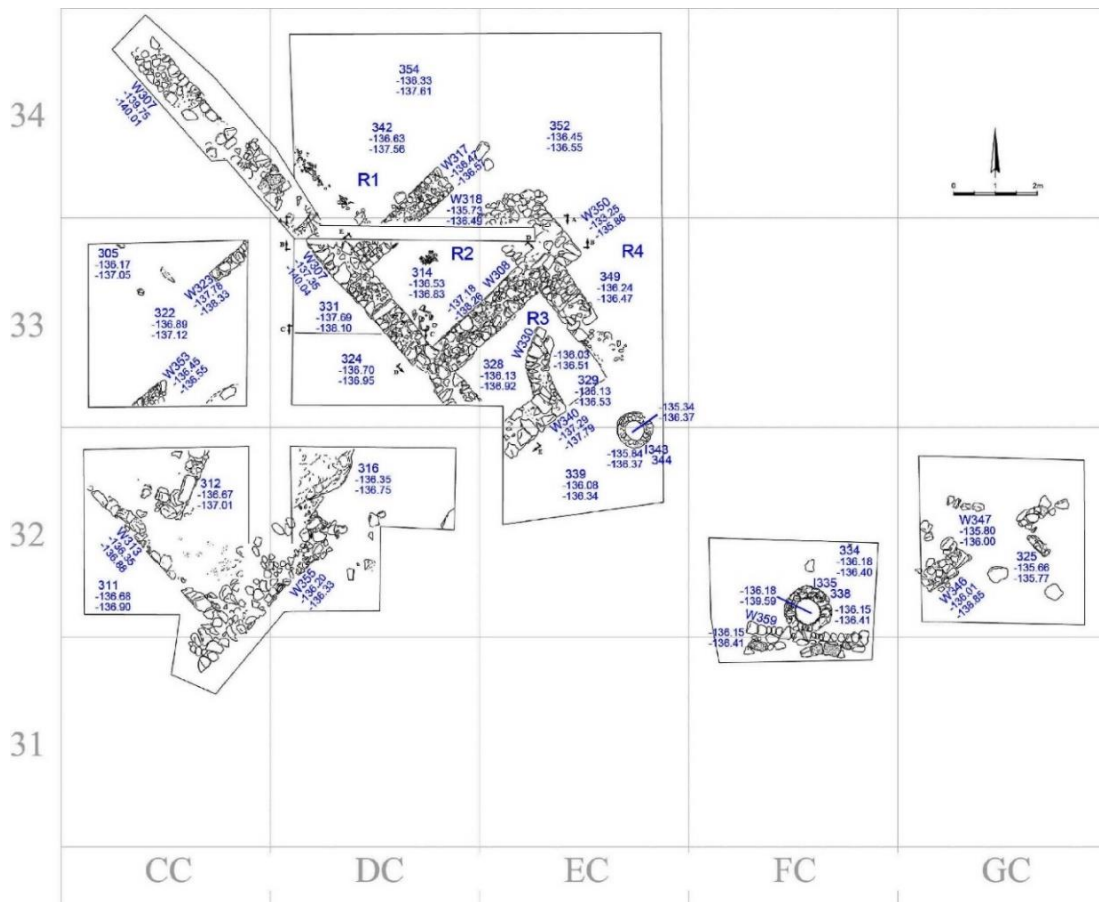


Figure 4. Plan of Tell İztabba (East), Area C of the German-Israeli Tell İztabba Excavation Project (Locus 324 is in Square DC33) ©German-Israeli Tell İztabba Excavation Project).



Figure 5. Area C, left) W307, during excavations, looking east; right) Locus 324 (Square DC33) during excavations, looking north ©German-Israeli Tell İztabba Excavation Project).

2. TECHNOLOGICAL BACKGROUND

2.1. Mortar and plaster building materials

Mortar is an artificial heterogeneous material used in buildings and constructions to fill the gaps between bricks and other building materials. It is a composite material consisting of an inorganic binder, such as lime (calcium carbonate, CaCO_3), which is used as a matrix, mixed with aggregates and/or sand (SiO_2) particles and water and it is used as a paste which is afterward dehydrated (Vázquez de Ágredos-Pascual *et al.*, 2019, pp. 182–183; Arizzi and Cultrone, 2021). The main function of the matrix is to join the embedded aggregate and/or sand particles together, whereas the embedded particles are added to achieve volume stability during drying and to increase the mechanical resistance of the dried mortar (Arizzi and Cultrone, 2021).

Plaster is a building material used for the shielding and decorative coating of walls. Plaster is normally composed of calcium carbonate, made of hydrated lime and calcite dust, embedded aggregates and sometimes mixed with white powder of gypsum, calcium sulphate hemihydrate ($\text{CaSO}_4 \cdot 2\text{H}_2\text{O}$) mineral (Ali and Elrahim, 2021, p. 47; Arizzi and Cultrone, 2021). Gypsum was added to create a smooth surface ready for coloring with brushes and oxides (Ali and Elrahim, 2021, p. 47). Limestone is a calcium carbonate sedimentary rock. It is among the most common building materials particularly in the Mediterranean region (Linn, 2017, p. 776). Limestone often contains other components, such as organic remains, rock fragments, and other minerals, such as clay minerals (hydrated aluminium phyllosilicates), dolomite [$\text{CaMg}(\text{CO}_3)_2$], ankerite $\text{Ca}(\text{Fe}, \text{Mg}, \text{Mn})(\text{CO}_3)_2$, siderite (FeCO_3), and quartz (SiO_2), as well as sulphates or sulphides (Arizzi and Cultrone, 2021; Szczepaniak, 2014). The presence of Si and Al in mortar and plaster materials often indicates that calcite (CaCO_3) fragments were mixed with slaked lime $\text{Ca}(\text{OH})_2$ (Apostolaki *et al.*, 2006, p. 731; Rao *et al.*, 2011). The mortar and plaster materials contain embedded aggregate minerals, such as quartz, potassium feldspar (KAlSi_3O_8), clinopyroxene [with general formula of $(\text{Ca}, \text{Mg}, \text{Fe}, \text{Na})(\text{Mg}, \text{Fe}, \text{Al})(\text{Si}, \text{Al})_2\text{O}_6$], and hematite (Klempan *et al.*, 2017, p. 1078).

2.2. Common wall painting pigments used during antiquity

During antiquity various pigments were used to create wall decorations (Table 1), which decorated public spaces, palaces, houses and tombs (Amadori *et al.*, 2015; Aquilia *et al.*, 2012; Barone *et al.*, 2018; Buzgar *et al.*, 2013; Crupi *et al.*, 2018; Di Stefano and Fuchs, 2011; Delaney *et al.*, 2017; Elias *et al.*, 2006; Fedorov and Samoylov, 2019; Fermo *et al.*, 2013; Fostiridou *et al.*, 2016; Gajić-Kvaščev *et al.*, 2012; Guirdzhiiska *et al.*, 2017; Gutman *et al.*, 2016; Holakooei *et al.*, 2015; Iordanidis *et al.*, 2014; Kakoulli, 2002; Klempan *et al.*, 2017; Linn, 2017; Mateos *et al.*, 2015; Mateos *et al.*, 2018; Mazzocchin *et al.*, 2003; Miriello *et al.*, 2021; Mortimore *et al.*, 2004; Olivares *et al.*, 2013; Piovesan *et al.*, 2016; Radpour *et al.*, 2019; Roebroeks *et al.*, 2012; Rozenberg, 2014; Sabbatini *et al.* 2000; Siddall, 2018; Szczepaniak, 2014; Van der Weerd *et al.*, 2004; Westlake *et al.*, 2012; Winter, 1983). The term “earth pigments” in the literature commonly refers to inorganic, naturally occurring minerals that are used as colorants, for instance naturally occurring ochres and green earth pigments (Marketou *et al.*, 2019; Radpour *et al.*, 2019). The term ochre (Table 1) refers to earth pigments made of rocks that contains iron oxide or iron hydroxide mixed with varying amounts of other materials such as clay and sand. The selection of particular pigments may have reflected a personal choice and/or common taste during a particular period. Yet, the selection of specific pigments may also have resulted from geographical limitations, the availability of raw materials in a particular region, along with economic considerations during a specific period (Apostolaki *et al.*, 2006, p. 729; Radpour *et al.*, 2019).

When archaeological wall paintings are studied, one of the most significant matters is the identification of the pigments that were used. Such characterization can provide valuable archaeological, ethnographical, anthropological and technological information concerning the local palette of pigments available in a certain region, as well as wider scale data of trade relations and trends in more distant regions (Amadori *et al.*, 2021; Dayet, 2021; Gutman *et al.*, 2016). Such data may also increase our understanding of the methods of color production and application as well as wall painting techniques during the period (Gutman *et al.*, 2016, p. 184).

Table 1. Common wall painting pigments that were used during antiquity.

| Color | Pigment | Formula | Description and information | References |
|---------------|---|---|---|--|
| White | Whiting chalk (also lime white) | Calcium carbonate, CaCO ₃ | A carbonate sedimentary rock. | Fermo et al., 2013; Gutman et al., 2016; Kakoulli, 2002; Linn, 2017; Szczepaniak, 2014. |
| | White gypsum | Calcium sulphate dihydrate mineral, CaSO ₄ · 2H ₂ O | Often used as white pigments during the entire period of ancient Egypt. | Di Stefano and Fuchs, 2011. |
| | Bone white | Calcium phosphate, Ca ₃ (PO ₄) ₂ | Made of bone ash. | Kakoulli, 2002. |
| | Kaolinite | Al ₂ Si ₂ O ₂ (OH) ₄ | White to cream clay mineral. | Kakoulli, 2002; Westlake et al., 2012. |
| | Potassium alum | KAl(SO ₄) ₂ · 12H ₂ O | Described by Pliny the Elder as alumen. | Delaney et al., 2017; Fedorov and Samoylov, 2019. |
| | Lead white (hydrocerussite) | 2PbCO ₃ · Pb(OH) ₂ | Milky white to gray mineral. | Kakoulli, 2002; Mazzocchin et al., 2003; Westlake et al., 2012. |
| | Celestite (strontium sulphate) | SrSO ₄ | White to blue mineral. | Kakoulli, 2002. |
| Red | Red ochre | Haematite, α-Fe ₂ O ₃ , mixed with different quantities of clay and sand. | Bright to dark red natural earth pigment. | Aquila et al., 2012; Elias et al., 2006; Gutman et al., 2016; Kakoulli, 2002; Mazzocchin et al., 2003; Mortimore et al., 2004; Roebroeks et al., 2012; Sabbatini et al., 2000. |
| | Hematite | Purest iron oxide, Fe ₂ O ₃ | Dark purple-red color. | Linn, 2017; Siddall, 2018. |
| | Cinnabar | Mercury(II) sulphide, HgS | A bright cherry to brick-red mineral, which is not very abundant in the earth's crust. | Fermo et al., 2013; Gajić-Kvašćev et al., 2012; Iordanidis et al., 2014; Kakoulli, 2002; Linn, 2017. |
| | Realgar | α-As ₄ S ₄ | Red to orange-yellow in color. | Di Stefano and Fuchs, 2011; Kakoulli, 2002. |
| | Vanadinite | Pb ₅ (VO ₄) ₃ Cl | A rare mineral with red to brownish-yellow color. | Holakooei et al., 2015; Kakoulli, 2002. |
| Red lead | Lead(II,IV) oxide, Pb ₃ O ₄ | Red with bright tones of pink and orange. This pigment was used in the Roman period. | Holakooei et al., 2015; Westlake et al., 2012. | |
| Yellow | Yellow ochre | Goethite, iron oxide hydroxide α-FeO(OH) | Yellowish-reddish to dark brown or black color. | Elias et al., 2006; Gutman et al., 2016; Fermo et al., 2013; Kakoulli, 2002; Mazzocchin et al., 2003. |
| | | Limonite, hydrated iron hydroxide, FeO · OH · nH ₂ O | Limonite is a mixture of several iron-containing minerals among them goethite (as a main component), akageneite, lepidocrocite, and jarosite. | |
| | | Potassium jarosite, KFe ₃ (SO ₄) ₂ (OH) ₆ | Yellowish-brown color. | |
| | Orpiment | As ₂ S ₃ | Transparent bright orange-yellow mineral formed in volcanic fumaroles and as a hot-springs deposit. | Di Stefano and Fuchs, 2011; Kakoulli, 2002. |
| | Sulphur flower | α-S | Bright yellow mineral. | Kakoulli, 2002. |
| Wulfenite | PbMoO ₄ | Yellow, orange-yellow, and honey-yellow. | Holakooei et al., 2015. | |
| Brown | Brown ochre | Haematite, α-Fe ₂ O ₃ , and/or goethite, FeO(OH), and often magnetite, Fe ₃ O ₄ | Partly hydrated iron oxide. | Elias et al., 2006; Fermo et al., 2013; Kakoulli, 2002; Mortimore et al., 2004; Piovesan et al., 2016. |
| | Raw umber | Fe ₂ O ₃ · MnO ₂ | Natural brown to reddish-brown earth pigment. | Kakoulli, 2002. |
| Black | Charcoal black | Carbon | One of the oldest known pigments. It was produced by intensely heating wood in a limited oxygen environment to remove water residues. | Ali and Youssef, 2020; Gutman et al., 2016; Iordanidis et al., 2014; Kakoulli, 2002; Klempner et al., 2017; Maz- |

| | | | | |
|--------------|----------------------|--|--|---|
| | Carbon black | Carbon | Produced by the partial burning of heavy petroleum products. | zocchin <i>et al.</i> , 2003; Olivares <i>et al.</i> , 2013; Sabbatini <i>et al.</i> 2000; Van der Weerd <i>et al.</i> , 2004; Winter, 1983. |
| | Bone black | Carbon + Ca ₃ (PO ₄) ₂ | Charcoal produced by heating bones of animals in the presence of a minimal amount of oxygen. | |
| | Vegetable bone black | Carbon + K ₂ CO ₃ | Formed by heating carbon of vegetable origin. | |
| | Pyrolusite | MnO ₂ | Black to lighter gray. | Buzgar <i>et al.</i> , 2013; Westlake <i>et al.</i> , 2012. |
| | Jacobsite | MnFe ₂ O ₄ | Black to dark brown. | Buzgar <i>et al.</i> , 2013. |
| Blue | Egyptian blue | Calcium copper silicate, CaCuSi ₄ O ₁₀ | Between light blue and dark sky blue. | Ali and Elrahim, 2021; Amadori <i>et al.</i> , 2015; Fostiridou <i>et al.</i> , 2016; Mateos <i>et al.</i> , 2015; Piovesan <i>et al.</i> , 2016. |
| Green | Malachite | Copper carbonate hydroxide mineral, CuCO ₃ · Cu(OH) ₂ | Between bright and dark green. | Ali and Youssef, 2020; Amadori <i>et al.</i> , 2021; Kakoulli, 2002; Mateos <i>et al.</i> , 2015. |
| | Green gypsum | Hydrated calcium sulphate, CaSO ₄ · 2H ₂ O | Bright green. | Mateos <i>et al.</i> , 2015. |
| | Green earth | Celadonite, K(Mg,Fe)(Fe,Al)Si ₄ O ₁₀ (OH) ₂ | Between bright and dark green, with an olive tone. | Kakoulli, 2002; Linn, 2017. |
| | Conicalcrite | Calcium copper arsenate, CaCuAsO ₄ (OH) | Grass-green to yellowish green. | Kakoulli, 2002. |
| | Serpentine green | Mg ₃ Si ₂ O ₅ · (OH) ₄ | Between bright and dark green. | Kakoulli, 2002. |

2.3. The use of iron oxides as pigments

Metal oxides are found naturally in rocks and soils and therefore have been used since prehistoric periods as pigment because of their abundance, stability, and color diversity (Table 1). For example, red ochre (hematite-rich, Fe₂O₃) and yellow ochre [goethite-rich, α-FeO(OH)] pigments were among the first colors that were used in antiquity by pre-historic artists to paint on cave walls (Olivares *et al.*, 2013, p. 1356; Roebroeks *et al.*, 2012, p. 1889; Román *et al.*, 2015, p. 84; Sajó *et al.*, 2015). Iron minerals were often used during ancient times since they are very abundant above the earth's surface, and because their main components, iron oxides and oxy-hydroxydes, are characterized by deep colors with a beautiful appearance, good coating properties and long-term durability. Ochre pigments are composed of various minerals and contain varying amount of iron oxide or oxy-hydroxyde, between 5–10 wt% to upwards of 90 wt% (Dayet, 2021). There is also evidence of prehistoric use of ochre pigments produced by iron-oxidizing bacteria (FeOB), with needle shaped structures probably connected to iron-oxidizing bacterial activities (Garilli *et al.*, 2020). Goethite is a yellow to orange-brown pigment, with an orthorhombic crystal system, which transforms into red, dark red and red-brown hematite (α-Fe₂O₃) due to a dehydration process (2α-FeOOH → α-Fe₂O₃ + H₂O) at 260–300 °C (Dayet, 2021; de Faria and Lopes, 2007, p. 117; Garilli *et al.*, 2020; Marcaida *et al.*, 2017, p. 3854; Wadley, 2009, p. 166). Moreover, when the heating process of yellow or brown ochre color takes place under a fire that lasts for several

hours, the pigment transforms into a red color at underground temperature above 250 °C (Wadley, 2009, p. 169). Hematite, with a hexagonal crystal system, is primarily formed as nano of micro domains, which merge at higher temperatures leading to a further crystalline compound (De Faria and Lopes, 2007, p. 117). Red ochre is a ubiquitous mineral in natural soils (Aquila *et al.*, 2012, p. 233; Mortimore *et al.*, 2004, p. 1179; Sajó *et al.*, 2015, p. 5). Red ochre pigment is often found at archaeological sites in the southern Levant (Tsatskin and Gendler, 2016, p. 284). A red ochre pigment was identified near various fire-related features in the Terra Rossa soil near the Kfar HaHoresh Neolithic site located in the Lower Galilee, Israel after characterization of the pigment by color catalogues, X-ray diffraction (XRD), X-ray fluorescence (XRF), and Fourier transform infrared (FTIR) analyses (Tsatskin and Gendler, 2016). The iron concentration and the iron-oxide crystalline grain size affects the hue of the red ochre pigment (Klempan *et al.*, 2017, p. 1091; Wadley, 2009, p. 166). For example, 1–2 μm goethite crystalline grains results in yellow hue, whereas 0.2 μm grains result in brown pigment (Wadley, 2009, p. 166). Presence of Cl in ochre pigments is usually related to a local occurrence of chlorinated salts (Amadori *et al.*, 2015, p. 187). In order to get bright red, ochre pigments may be mixed with St. John white (calcium carbonate) (Sabbatini *et al.* 2000, p. 123). Sometime white lead was mixed with yellow ochre pigment in order to achieve a lighter hue of yellow, or massicot (PbO) lead (II) oxide mineral was used as a yellow pigment (Asderaki-Tzoumerkoti and

Doulgeri-Intzesiloglou, 2010, p. 5). Brown ochre pigment is associated with both red and yellow ochre (Marketou et al., 2019; Piovesan et al., 2016, pp. 440–441). However, lower iron content is presented in the brown ochre pigment compared to the red ochre (Marketou et al., 2019). Moreover, magnetite (Fe_3O_4), the black iron oxide, is frequently also presented in brown ochres (Piovesan et al., 2016, pp. 440–441).

2.4. *The fresco and secco painting techniques*

Palaces and houses in Ancient Greece and Rome were frequently beautifully decorated with wall paintings (Rozenberg, 2014, p. 120). The two most commonly used wall painting decoration methods were the fresco and secco techniques (Cerrato et al., 2021; Rozenberg, 2014, p. 123). The word fresco originates from the Italian expression “*buon fresco*”, which means “really fresh” (wet). Fresco is a technique of wall painting whereby the paint is made by mixing ground pigment powder with a water medium to create a suspension; next the painting is created on top of fresh wet plaster made of hydrated lime [$\text{CaO} + \text{H}_2\text{O} \rightarrow \text{Ca}(\text{OH})_2$] and embedded aggregates. Dissolved lime diffuses from the plaster material into the painted layer and acts as a binder (Ali and Youssef, 2020, p. 50; Apostolaki et al., 2006, pp. 729–730; Coccato et al., 2021, p. 3; Duran et al., 2011, p. 2373; Westlake et al., 2012, p. 1414). Therefore, the use of the fresco technique may be detected by light microscope observation of the cross-section of the wall painted samples due to the absence of a notable sharp separation between the plaster material and the painting layer (Amadori et al., 2015, pp. 187, 190; Gutman et al., 2016, p. 200; Taglieri et al., 2019, p. 161). The absence of some organic binder in the decorated areas indicates that the technique used to create the mural was fresco (Vázquez de Ágredos-Pascual, 2019, p. 182).

Unlike fresco, secco means “on dry surface”, where in this type of mural painting the paint is applied on top of dry plaster surfaces with pigments mixed in an organic binding medium. The main difference between the fresco and secco methods is that the fresco wet plaster absorbs the pigments of the paint and when the walls are dry, the painting becomes part of their surface, whereas in the case of secco paintings the pigments were applied on top of the dry walls, coating their exterior surface. The use of the secco technique may be observed by light microscopy of the samples’ cross-section due to the presence of a distinguishable separation between the plaster and the painting layer (Gil-Torrano et al., 2019, p. 7).

Both fresco and secco techniques were ubiquitous in ancient wall paintings. Moreover, many wall paintings in Ancient Greece and Rome were done by using

a combination of those two techniques, where the initial painting was done using the fresco method and then details were often added later by using the secco technique (Apostolaki et al., 2006, pp. 729–730; Rozenberg, 2014, p. 123). Despite the differences between fresco and secco, in both techniques it was common to use metal oxides as pigments during the Hellenistic and Roman periods, as shown below.

2.5. *The use of pigments in the Hellenistic and Roman periods*

Hellenistic Terracotta figurines from Pherai (Greece) were studied by Asderaki-Tzoumerkioti and Doulgeri-Intzesiloglou (2021) in order to analyze the raw materials of the pigments and found that just a few pigments, mainly black and red, were sometimes applied directly on the clay body, whereas most decorative pieces had a white film covering of the ceramic body, and only on top of it were the colors painted. Their results indicated that the white substrate was made of three kinds of white: (1) calcite (trigonal crystal system) and/or aragonite (orthorhombic crystal system), which are dissimilar non-silicate rock crystal forms of calcium carbonate (CaCO_3), (2) gypsum calcium sulfate dihydrate mineral [$\text{CaSO}_4 \cdot 2(\text{H}_2\text{O})$], and (3) white lead carbonate complex salt [$\text{Pb}_3(\text{CO}_3)_2(\text{OH})_2$]. Calcite and aragonite minerals were very common white color pigments, found either as the major component of the substrate or mixed with additional pigments to create lighter hues (Asderaki-Tzoumerkioti and Doulgeri-Intzesiloglou, 2010, p. 8; Fermo et al., 2013, p. 1113; Gutman et al., 2016, p. 201; Kakoulli, 2002, p. 64; Szczepaniak, 2014, p. 29). In addition to calcium carbonate, gypsum calcium sulfate dehydrate and white lead, other white pigments that were used during antiquity are bone white, kaolinite, potassium alum and celestite (Delaney et al., 2017, p. 8; Di Stefano and Fuchs, 2011, p. 234; Fedorov and Samoylov, 2019, p. 32; Kakoulli, 2002, p. 64; Mazzocchin et al., 2003, p. 567; Westlake et al., 2012, p. 1414).

Carbon-based black pigments, such as charcoal black, carbon (coal) black, bone black and vegetable bone black were widely used during antiquity (Table 1). For example, Klempan and his colleagues (2017) studied pigments retrieved from the Etruscan wall paintings at Caere, Italy, dated to the Hellenistic period, and discovered that the black color was charcoal black (Klempan et al., 2017, p. 1087). When large amounts of phosphorus and calcium are detected in a black paint, the pigments are associated with bone black or with ivory black (Duran et al., 2011, p. 2375). Gray color was achieved by mixing black pigments, such as carbon-based black, with calcite powder (Iordanidis et al., 2014, p. 2717).

Dark and light olive green tones, with hues between yellow-green and deep green, were produced by many combinations of yellow ochre, green earth, Egyptian blue and pyrolusite Mn-based black pigment (Radpour *et al.*, 2019).

There are many examples in the literature of the use of pigments in the Mediterranean during the period between the third century BCE and the second century CE. For example, Fostiridou and his colleagues studied the pigments of Hellenistic funeral figurines, dated between the third and second centuries BCE, and Roman funeral figurines, dated between the first and second centuries CE retrieved from tombs in the center of Thessaloniki, Greece. These figurines revealed the presence of red ochre, yellow ochre, cinnabar [mercury(II) sulfide (HgS)], Egyptian blue ($\text{CaCuSi}_4\text{O}_{10}$), and carbon-based black pigments, as well as the presence of calcite, dolomite and quartz (Fostiridou *et al.*, 2016, p. 453). At Tel Anafa, Israel, red and yellow pigments showed high levels of iron; two pink samples were made of white-lead with mercury enrichment, while the green pigment was made of copper-oxide (Verdigris) and black of carbon-based material (Kidd, 1999, pp. 9–10; Kidd, 2018).

White calcium carbonate, red ochre, yellow ochre, brown ochre, and carbon-based black pigments were very common in Mediterranean wall paintings in Hellenistic- and Roman-period Greece. Yet, in some cases other pigments, such as Egyptian blue and green earth (celadonite), were also used. For example, examination of decorated graves of Etruscan Tarquinia, Italy, dated between the seventh and second centuries BCE, found that the pre-Roman wall paintings were painted with white calcite, red ochre, yellow ochre, and carbon-based black pigments; yet, other pigments, including green malachite pigment, Egyptian blue, lazurite violet (*Caeruleum Scythicum*) pigment, and red cinnabar were also used (Barone *et al.*, 2018, pp. 394–397). Hellenistic decorative wall paintings from Thracian fresco tombs found in south Bulgaria, dated to fourth-third centuries BCE, were painted with red and yellow ochres and with white calcite (Guirdzhiiska *et al.*, 2017, p. 431). Hellenistic period samples retrieved from the Etruscan wall paintings at Caere, Italy revealed the use of white calcite, charcoal black, red and yellow ochres, and Egyptian blue pigments (Klempan *et al.*, 2017, p. 1087). Analysis of wall paintings found in Hellenistic and Roman Paphos, Cyprus revealed that they were made of red ochre, yellow ochre, and chalk white pigments and black iron oxide was used as black pigment (Balandier *et al.*, 2017, p. 336). Analysis of colors from a pigment production site located at the ancient agora of Kos, Greece, dated to the late Hellenistic period (second half of the first century BCE), revealed that the red

pigment was attributed to hematite. However, two of the red samples also contained lead tetroxide in addition to the hematite. The yellow color was identified as yellow earth (goethite and quartz), but yellow jarosite was also detected. The brown pigments were produced by mixing different iron oxides. The blue pigment was identified as Egyptian blue, and the green color was made of green earth pigment produced of celadonic rock (Marketou *et al.*, 2019). Examination of red, brown, black, and green wall painting fragments from the archaeological site of Pompeii, Italy revealed the use of red, yellow and brown ochres, green earth, and charcoal as a black pigment (Miriello *et al.*, 2018). In situ examination of two mural paintings of the “House of Garden” in Pompeii identified various pigments, including lead white, yellow ochre, lead white mixed with yellow ochre in order to obtain light-yellow regions, red hematite, Egyptian blue and black carbon (Miriello *et al.*, 2021). In situ characterization of Pompeian blue, green, yellow and red pigments preserved in their original bowls revealed the use of Egyptian blue, green malachite pigment, yellow ochre, red ochre and cinnabar minerals (Marcaida *et al.*, 2018). The use of cinnabar pigment in Roman times was an indicator of richness, whereas red ochre, in contrast, was a much cheaper pigment (Marcaida *et al.*, 2018, p. 461). Analysis of wall painting samples retrieved from a Roman villa in Mošnje, located in the north-west of Slovenia and built in the first half of the first century CE, revealed the use of red and yellow ochres, green earth, lime white and carbon-based black pigments (Gutman *et al.*, 2016, p. 201). Analysis of Roman frescoes retrieved from the Villa dei Quintili, Rome, Italy, dated to the second century CE, identified the use of lime white, red ochre and yellow ochres, carbon black of vegetable origin, and Egyptian blue pigments (Crupi *et al.*, 2018, p. 422). Study of layered pigments from Roman wall paintings discovered in Caesarea, Israel from both domestic and public buildings, dated between the late first century CE and the third century CE, revealed the use of lime white, yellow and red ochres, hematite, cinnabar, red lake, carbon-based black, Egyptian blue, and green-earth pigments (Linn, 2017, p. 775). Analysis of decorative pigments from the walls of the Roman villa of El Ruedo in southern Spain, dated to the third to fifth centuries CE, revealed the use of red, orange, yellow and pink ochres, white calcite and carbon black, as well as Egyptian blue, green gypsum, and green earth (Mateos *et al.*, 2015, p. 19). Analysis of wall paintings from the Roman villa of Fuente Alamo in southern Spain revealed the use of lime white, red and yellow ochres, carbon-based smoke black, Egyptian blue and green earth pigments (Mateos *et al.*, 2018, pp. 19–22).

2.6. The characterization methods of wall painting pigments

A multidisciplinary archaeometric approach is essential in order to achieve information concerning the materials and techniques that were used for wall paintings during antiquity (Liritzis et al., 2020; Miriello et al., 2021, p. 258). Characterization of wall pigments should always start with macroscopic visual testing (VT) examinations in order to determine the condition of the decorated wall and the degree of damage, including cracks, notches, gaps and deposits, such as dirt, dust and soot (Ali and Youssef, 2020, p. 42). Successful study of pigments should include a combination of two main types of analyses: (1) mineralogical analyses and (2) total elemental analyses (Dayet, 2021). The most common methods used to identify a color palette, including pigments of lime white, red, yellow and brown ochres, carbon-based black, as well as other pigments such as the green earths, green gypsum, Egyptian blue, and others are XRF analysis, scanning electron microscope (SEM) analysis with energy dispersive spectroscopy (EDS), XRD, Raman spectroscopy, and FTIR spectroscopy (Amadori et al., 2021; Crupi et al., 2018, p. 423; Fostiridou et al., 2016, p. 453; Gil-Torrano et al., 2019, p. 5; Guirdzhiiska et al., 2017, p. 431; Gutman et al., 2016, p. 194; Holakooei et al., 2016; Linn, 2017, p. 776; Marcáida et al., 2017; Marketou et al., 2019; Mateos et al., 2018; Siddall, 2018; Taglieri et al., 2019, p. 158). Other methods for pigment identification are color catalogues, petrography combined with polarized light microscopy, infrared spectroscopy, pyrolysis-gas chromatography-mass spectrometry (Py-GC-MS), particle-induced X-ray emission (PIXE) analysis, neutron activation analysis (NAA), inductively coupled plasma and atomic emission spectroscopy (ICP-AES), inductively coupled mass spectrometry (ICP-MS, with laser ablation: LA-ICP-MS), X-ray Photoelectron Spectroscopy (XPS), High-resolution scanning electron microscopy (HRSEM), and transmission electron microscopy (TEM) (Arizzi and Cultrone, 2021; Dayet, 2021; Di Stefano and Fuchs, 2011; Garilli et al., 2020; Klempan et al., 2017; Liritzis et al., 2020; Piovesan et al., 2016; Tsatskin and Gendler, 2016). The mineralogical characterization can be done by XRD, Raman spectrometry, FTIR, petrography, as well as by thermogravimetry or Mössbauer spectrometry. SEM-EDS technique allows total elemental analysis, but it is also a main method for the identification of mineral phases on the surface of a sample according to its images in back scattered electron (BSE) mode, which highlights chemical contrasts in combination with EDS chemical analysis. Therefore, according to Dayet the most recommended method for pigment characterization is the SEM-EDS analysis. Yet, as in other

fields of materials characterization, the combination of several methods is always preferred in order to reduce the risk of misinterpretation of the phases and confusion between minerals. The recommended methods for elemental analysis of pigment materials are XRF, SEM-EDS, PIXE, NAA, ICP-AES, and LA-ICP-MS (Dayet, 2021).

3. EXPERIMENTAL METHODS

- (a) VT inspection of the samples retrieved from the wall painting plaster and pigments (Fig. 6) was carried out in order to examine the general condition of the samples and to detect visible characteristics and defects that may assist in understanding the manufacturing process.
- (b) In order to build a macroscopic level catalogue of the plaster and pigments retrieved from Tell İztabba and to be able to visually compare the pigments to the available literature, the sample surfaces were photographed in daylight by using a Canon 6D Camera, with EF 40 mm 1/2.8 STM Lens, as well as XIT Extension Macro Rings (65 mm) equipment.
- (c) XRF method for non-destructive testing (NDT) analysis is frequently used to determine the chemical composition of ancient plasters and pigments with characteristic detection limits of 0.01% for main elements and about 1–5 ppm for trace elements (Arizzi and Cultrone, 2021). This non-invasive technique can be applied in situ in order to identify inorganic compounds (Liritzis et al., 2020, p. 66). In order to obtain preliminary results of the composition of the plaster and pigments, chemical analysis was done by using a XLt-900 GOLDD (Thermo Scientific™ Niton) handheld (HH) XRF machine. This instrument is equipped with a 50 kV Target X-ray tube and 80 MHz real-time digital signal process. The irradiation area was circular (8 mm in diameter) and each measurement was performed for 60 seconds and measurements were done by means of the characteristic secondary X-rays emitted from the material as it was bombarded with high-energy X-rays. This tool is equipped with a Geometrically Optimized Large Area Drift Detector (GOLDD™) for better analysis of light elements (Mg-S). Yet, light elements such as carbon and oxygen could not be identified with this HH-XRF instrument due to strong absorption of X-rays owing to trapped air between the sample and the XRF detector (Duran et al., 2011, p. 2373). Therefore, the elemental concentrations based on the XRF results are presented here unnormalized (total elements composition is not 100

wt%). Moreover, in order to achieve reliable results with a portable HfH-XRF machine several factors must be taken into account, such as the correct calibration of the instrument and the surface roughness (Liritzis *et al.*, 2020, pp. 62, 66).

(d) Scanning Electron Microscope (SEM) analysis was preformed, including Energy Dispersive Spectroscopy (EDS) chemical analysis with an Environmental SEM. One of the main advantages of using ESEM for plaster and pigment characterization is that the samples do not need carbon or gold coating, as the examination is carried out under low vacuum mode conditions (Arizzi and Cultrone, 2021). The samples were characterized by a FEI Quanta 200FEG ESEM, equipped with an Everhart-Thonley secondary electron (SE) detector. Both SE and BSE modes were applied in order to inspect the pigments. The EDS analysis was performed with Si(Li) liquid-cooled Oxford X-ray detector. The decorated surface of the samples was first examined in the planar section (P-section). However, in order to better understand the technology that was used to paint the walls, samples were also ground in the transvers cross-section (T-CS) with 340–4000 silicon carbide grit papers and then examined by SEM. Such T-CS examination assisted in distinguish-

ing fresco from secco painting techniques (Coccatto *et al.*, 2021). In order to compare the EDS and XRF analyses results, the EDS analysis results are presented in their elemental composition and not as oxides.

(e) X-ray diffraction (XRD) analysis was applied to identify the crystalline phases of the brown paint. A large database exists and data interpretation is quite straightforward; nevertheless, peak overlap may occur. The analysis was performed with D8 Advance, Bruker diffractometer (435 mm diameter) designed for X-ray powder diffraction (XRPD) with theta-theta (Bragg-Brentano) and a 2.2 kW Cu sealed tube X-ray source, generating Cu K α radiation at a wavelength of 1.541 Å from a generator working condition of 40 kV and 40 mA and power stability better than 0.01%. A parallel beam of monochromatic X-ray radiation was created by the use of a Göbel mirror optics. The brown paint layer was peeled from Sample no. 6 by using a stainless steel scalpel and then the brown layer was crushed with an agate mortar to a fine powder that was examined by XRD. The sample was rotated to offer better sampling, with a 10°–100° range and a step size of 0.02°. The data achieved from XRD analysis was interpreted by using Bruker-DIF-FRAC.EVA software.

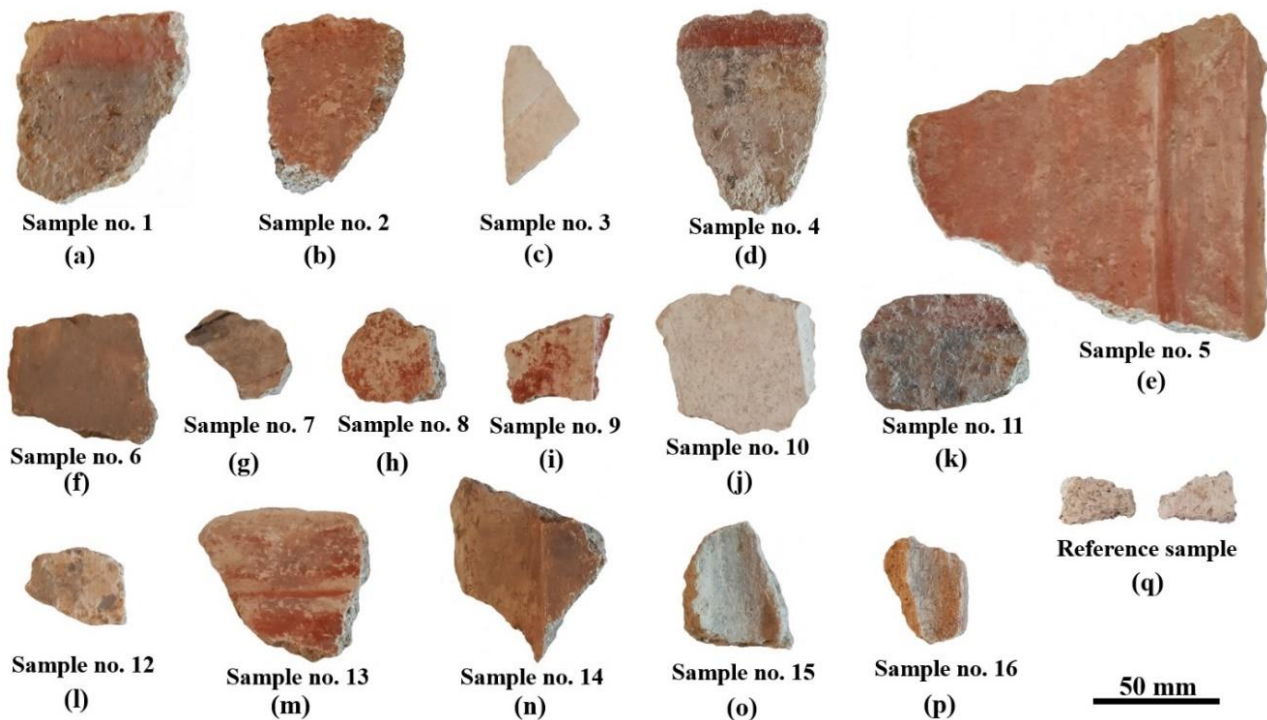


Figure 6. The wall fragments retrieved from the Tell Iztabba wall paintings: (a)–(p) samples 1–16, respectively; and (q) a reference sample.

4. RESULTS

Based on VT inspection of the Tell İztabba painted wall samples, a short description of the samples is given here. Sample no. 1 (Fig. 6a) includes a bright red strip on its upper parts, a thin layer of black color below it, and exposed plaster on the lower part of the sample. Sample no. 2 (Fig. 6b) is coated with bright red color. Sample no. 3 (Fig. 6c) is made of two layers of white plaster. Sample no. 4 (Fig. 6d) includes a red strip, below it a thin brown-gray strip, and below it yellow color on the right side and black areas on the left side, as well as areas of exposed plaster on both sides. Sample no. 5 (Fig. 6e) is coated with bright red color. Sample no. 6 (Fig. 6f) is coated with brown-gray color. The upper left side of Sample no. 7 (Fig. 6g) is covered with black and brown-gray strips; the central part reveals brown-gray color as well as exposed plaster and the right lower side is coated with bright red color. Samples no. 8 and 9 (Fig. 6h, 6i, respectively), are covered with bright red color and areas of exposed plaster. Sample no. 10 (Fig. 6j) is covered with two layers of white plaster. Sample no. 11 (Fig. 6k) includes remains of a red strip on its upper parts, yellow color on its right side, and black color and exposed plaster at the rest of the sample. Sample no. 12 (Fig. 6l) is composed of exposed plaster, as well as remains of yellow and black-gray colors. Sample no. 13 (Fig. 6m) is covered with red color and some areas of exposed plaster. Sample no. 14 (Fig. 6n) is covered with red pigment on the left and brown-gray pigment on the right. Sample no. 15 (Fig. 6o) is covered with areas of brown-gray color. The right side of Sample no. 16 (Fig. 6p) is covered with bright red and its left side covered with brown-gray color. A reference sample (Fig. 6q) is made of plaster taken from the Tell İztabba's walls.

4.1. *The white plaster from the painted walls of Tell İztabba (Area C, W307)*

VT inspection revealed that the base of all samples retrieved from the painted walls is made of plaster material (matrix) with embedded white, brown, gray, red, orange, yellow and black particles. The size of the embedded particles was up to 2 mm (Figs. 7b, 7i, 7p, 8a–c). Some of the samples include one layer of plaster, whereas others include two layers: a substrate layer (the lower layer) and a cover layer (the upper layer) (Fig. 8a–b). In all samples the area close to the paint was finer, smoother, and brighter, indicating that fewer embedded particles were used near the upper external surface of the plaster, and the external surface of the walls was probably smoothed with water (Fig. 7k, 7o). The back side of the plaster included a

coarse and rough surface (Figs. 7i, 8e), and perhaps had some mortar remains. The plaster was decorated with red, yellow, brown-gray, and black decorations (Figs. 6 and 7). Observation of the T-CS of Sample no. 4 revealed gradual transition (absence of a notable sharp separation) between the plaster material and the black and red painted layer (Fig. 8d), as typical of the fresco technique.

XRF analysis of the plaster substrate and plaster cover layers revealed that both were mainly composed of Ca (10.1–38.5 wt%), yet up to 13.3 wt% of Si and up to 12.4 wt% S were detected as well (Table 2). Up to 2.0 wt% of the elements Fe, Al, Cl, K, Ti, P, and Mn were also detected in the plaster samples (Table 2). The Si content was higher in the substrate plaster than in the upper plaster layers, probably resulting from the sand particles embedded in the substrate plaster matrix (Table 2).

SEM observation of the fine plaster's external surface revealed a relatively uniform surface (Fig. 9a–b). SEM observation of the T-CS of Sample no. 4 (BSE mode) revealed a gradual layer between the plaster and the red painted layer (Fig. 9c), as typical of the fresco technique. Higher SEM magnifications revealed a crystalline microstructure as well as sponge morphology (Fig. 9d–g). SEM observation of the coarse plaster substrate material revealed a rougher surface than the cover layer plaster material, with crystal grains of 2–8 μm in size (Fig. 8f–g). The crystalline microstructure of the fine cover plaster near the paint includes grains of 1–5 μm in size as well as smaller grains of 200–600 nm in size (Figs. 9, 10), which may hint that the plaster was made of calcite fragments mixed with slaked lime (Apostolaki et al., 2006, p. 731).

SEM-EDS analysis revealed that the coarse plaster substrate composition is 26.9–34.2 wt% Ca, 50.5–58.4 wt% O, up to 17.2 wt% C, 2.3–3.6 wt% Si, and up to 0.8 wt% of the elements S, Fe, Al, Mg, Na, Cl and K (Table 3, Fig. 8f–g). SEM-EDS analysis of the fine plaster cover (Figs. 9) revealed a similar composition of 28.2–40.4 wt% Ca, 45.4–51.5 wt% O, 9.9–13.7 wt% C, 0.9–11.1 wt% Si, 0.3–12.3 wt% S, up to 1.3 wt% of the elements Fe, Al, Mg, Na, Cl and K (Table 3, Fig. 9b–e, 9f). The analysis results show that the coarse plaster and the fine plaster are mainly composed of CaCO_3 . The EDS results (Table 3) are in good agreement with the XRF results of the plaster (Table 2). SEM-EDS analysis of the white particle shown in Fig. 8c (T-CS, arrow) revealed it is composed of 27.3 wt% Ca, 20.2 wt% S, 52.3 wt% O, and 0.2 wt% Si (Table 3), indicating that the embedded white particle is a calcium sulphate mineral, typical of white gypsum pigment (Table 1).

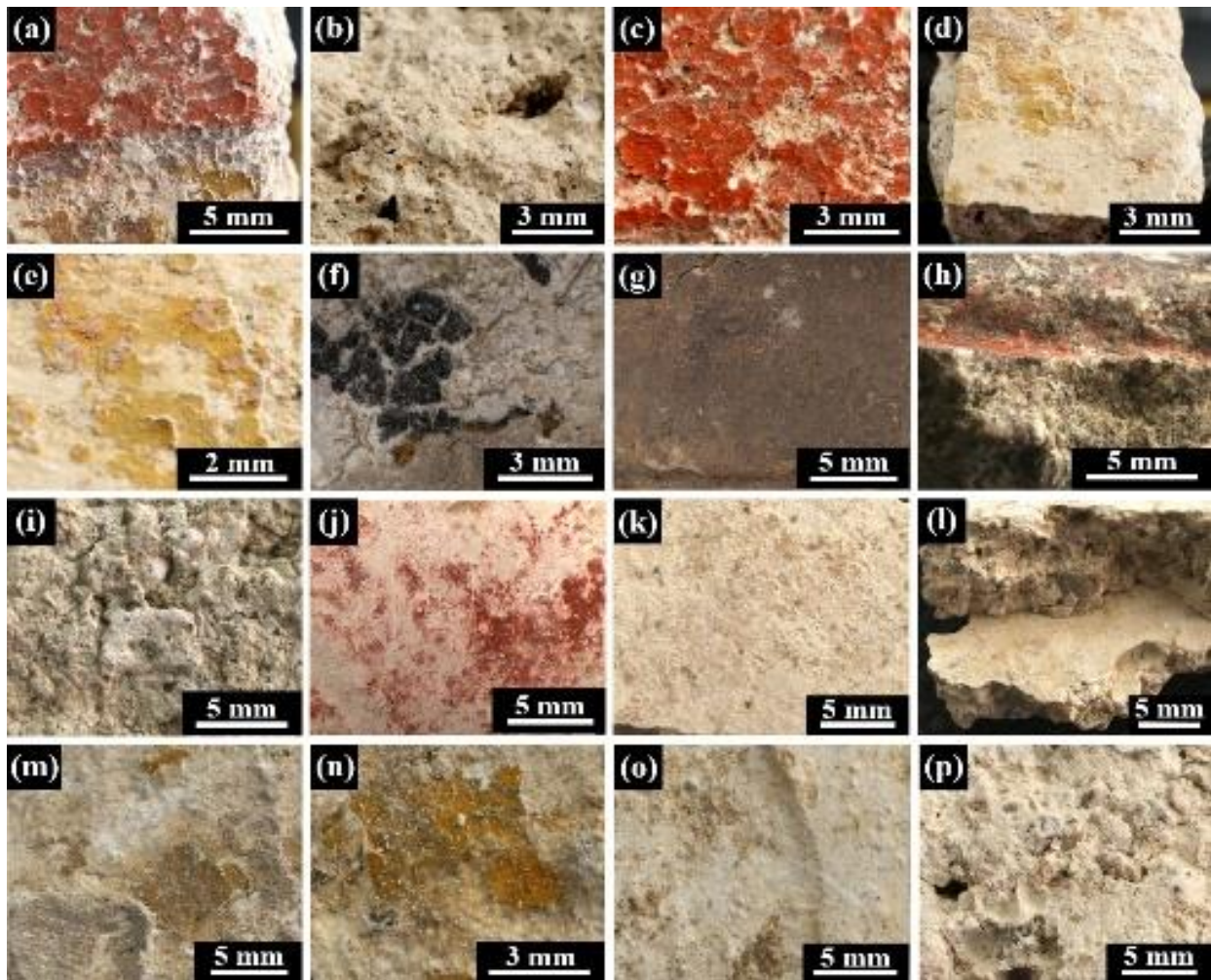


Figure 7. A catalogue of the plaster and pigments retrieved from the Tell Iztabba wall paintings (Canon 6D camera): (a) Sample no. 4, showing dark red, brown-gray, and yellow pigments (P-section); (b) rough plaster substrate at the back of Sample no. 4 (P-section); (c) dark red pigment (Sample no. 4, P-section); (d)-(e) yellow pigment surrounded by plaster (Sample no. 4, P-section); (f) black pigment surrounded by plaster material (Sample no. 4, P-section); (g) brown-gray pigment (Sample no. 6, P-section); (h) brown-gray pigment at the center of Fig. 7h and a step with red pigment (Sample no. 6, isometric view); (i) rough plaster at the back of Sample no. 8 (P-section); (j) light red pigment surrounded by plaster material (Sample no. 8, P-section); (k) upper layer of plaster (Sample no. 10, P-section); (l) the upper layer and the lower layer of plaster (Sample no. 10, isometric view); (m) yellow pigment at the center of Fig. 7m and gray pigment at the lower left part of the image, surrounded by plaster (Sample no. 11, P-section); (n) yellow pigment (Sample no. 11, P-section); (o) fine plaster (reference sample); and (p) rough plaster (back of the reference sample).

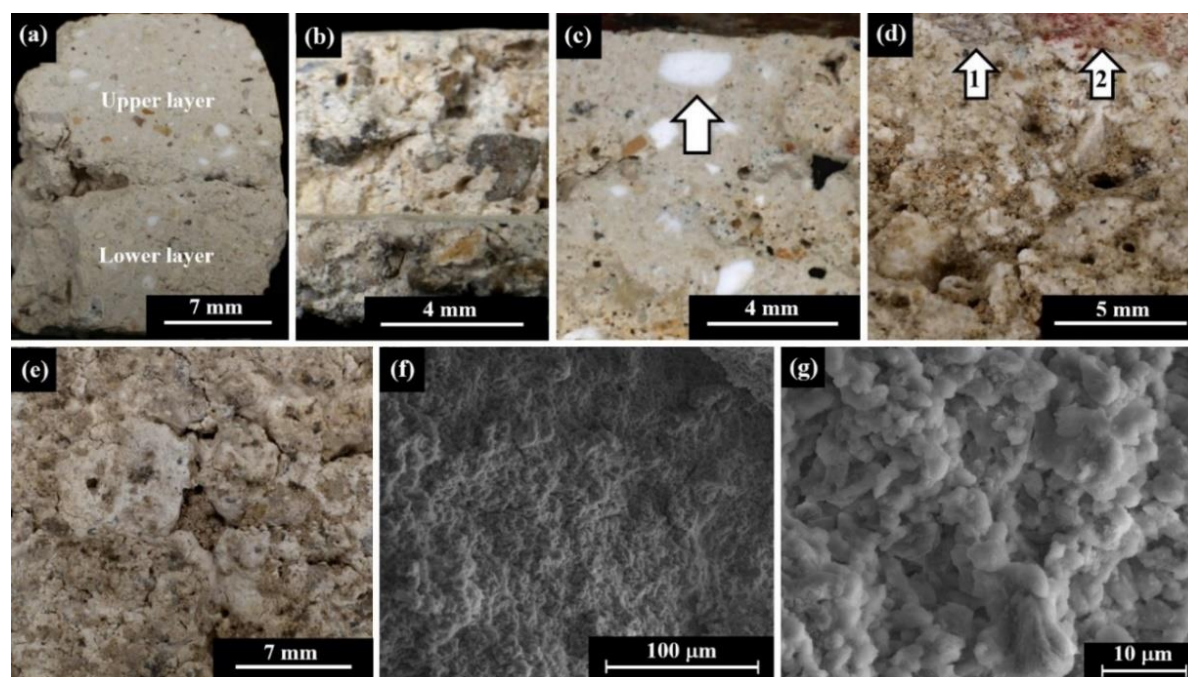


Figure 8. Images of the plaster: (a) two layers of plaster, where layer 1 is the substrate layer and layer 2 is the cover layer below the paint (Sample no. 4, polished T-CS), where the upper part of layer 2 is finer than the rest of the plaster with fewer embedded particles; (b) two layers of plaster (Sample no. 10, T-CS); (c) a white inclusion identified by EDS analysis as calcium sulphate dihydrate mineral (white arrow, Sample no. 4, T-CS); (d) a diffusion of pigments into the plaster layer, where arrow 1 shows black pigment and arrow 2 shows the red pigment (Sample no. 4, T-CS); (e) plaster at the back side of Sample no. 8 (P-section); (f) SEM observation of the plaster substrate (reference sample, P-section); and (g) SEM higher magnification showing crystals of 2–8 μm in size (reference sample, plaster substrate, P-section).

Table 2. XRF chemical analysis of the plaster (P-section).

| Sample description | Locus | Composition weight percentage (wt%) | | | | | | | | | | |
|---|-------|-------------------------------------|------|------|-----|-----|-----|-----|-----|-----|-----|--|
| | | Ca | Si | S | Fe | Al | Cl | K | Ti | P | Mn | |
| Sample no. 1, coarse substrate plaster | 324 | 21.7 | 2.2 | 9.1 | 0.5 | - | 0.1 | 0.3 | - | 0.1 | - | |
| Sample no. 2, plaster | 324 | 28.9 | 5.2 | 0.5 | 1.4 | 0.8 | 0.1 | 0.6 | 0.2 | 0.3 | 0.2 | |
| Sample no. 3, plaster with white hue | 324 | 11.1 | 13.3 | 0.4 | 3.4 | 1.7 | 0.2 | 2.5 | 0.4 | 0.4 | - | |
| Sample no. 4, coarse substrate plaster | 326 | 24.9 | 4.4 | 5.6 | 1.0 | 0.5 | 0.1 | 0.5 | 0.2 | 0.3 | - | |
| Sample no. 5, coarse substrate plaster, area 1 | 326 | 16.0 | 2.5 | 0.1 | 1.4 | - | - | 0.5 | 0.2 | 0.3 | - | |
| Sample no. 5, coarse substrate plaster, area 2 | 324 | 10.1 | - | - | 0.8 | - | - | 0.3 | 0.1 | 0.6 | - | |
| Sample no. 6, coarse substrate plaster | 326 | 26.7 | 5.4 | 0.3 | 1.4 | 0.8 | 0.1 | 0.7 | 0.2 | 0.3 | - | |
| Sample no. 7, fine and smooth plaster | 324 | 25.1 | 4.7 | 4.9 | 1.1 | 1.0 | 0.1 | 0.5 | 0.2 | 0.2 | - | |
| Sample no. 7, fine and smooth plaster with white hue | 324 | 25.2 | 5.3 | 7.0 | 0.8 | 0.8 | 0.2 | 0.5 | 0.2 | 0.2 | - | |
| Sample no. 8, fine and smooth plaster | 324 | 31.4 | 3.6 | 1.1 | 1.0 | 0.7 | 0.1 | 0.4 | 0.1 | 0.2 | 0.1 | |
| Sample no. 9, fine and smooth plaster | 324 | 35.5 | 2.7 | 0.7 | 1.6 | 1.1 | 0.1 | 0.3 | - | 0.2 | - | |
| Sample no. 9, coarse substrate plaster | 324 | 22.4 | 5.5 | 1.6 | 1.6 | 0.7 | 0.1 | 0.7 | 0.2 | 0.3 | - | |
| Sample no. 10, fine and smooth plaster with white hue | 324 | 38.5 | 1.8 | 0.2 | 0.6 | - | 0.1 | 0.2 | - | 0.1 | - | |
| Sample no. 10, coarse substrate plaster | 324 | 21.9 | 6.2 | 1.5 | 1.7 | 0.9 | 0.1 | 0.8 | 0.2 | 0.2 | - | |
| Sample no. 11, coarse substrate plaster | 324 | 26.3 | 2.8 | 6.1 | 0.6 | - | - | 0.3 | 0.1 | 0.2 | - | |
| Sample no. 12, fine and smooth plaster | 324 | 23.8 | 2.3 | 10.5 | 0.7 | - | - | 0.3 | 0.1 | 0.2 | - | |
| Sample no. 12, fine and smooth plaster with white hue | 324 | 23.3 | 3.6 | 12.4 | 0.5 | - | - | 0.3 | - | 0.1 | - | |
| Sample no. 13, coarse substrate plaster | 326 | 23.5 | 6.2 | 0.5 | 2.0 | 1.1 | 0.1 | 0.8 | 0.3 | 0.3 | - | |

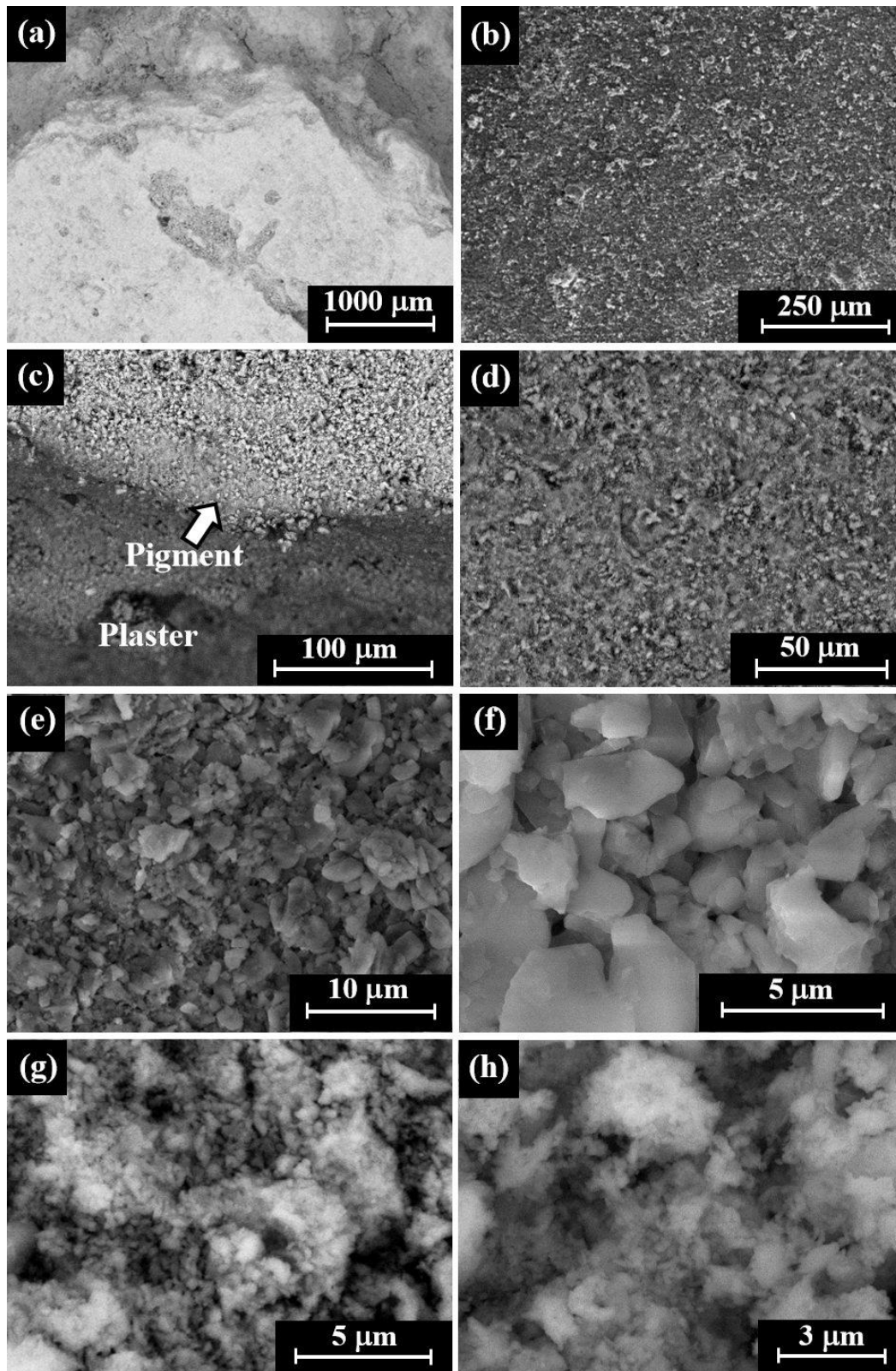


Figure 9. SEM images of the plaster: (a) general view of the white fine exterior surface of the reference sample in Fig. 6q (BSE mode, P-section); (b) higher magnification of the Fig. 9a (SE mode); (c) the interface between the plaster (dark area) and red pigment, showing the presence of pigment particles within the plaster (bright particles according to BSE mode, T-CS, Sample no. 4); (d) higher magnification of the area shown in Fig. 9b (BSE modes, P-section, reference sample), (e) area of crystalline microstructure (SE mode, Sample no. 4, P-section); (f) higher magnification of Fig. 9e showing grains of 1–4 μm in size; (g) crystalline microstructure and sponge morphology (reference sample, BSE mode); and (h) higher magnification showing sponge morphology and crystalline grains of 1–5 μm , as well as smaller crystalline grains of 200–400 nm in size (SE and BSE modes, respectively).

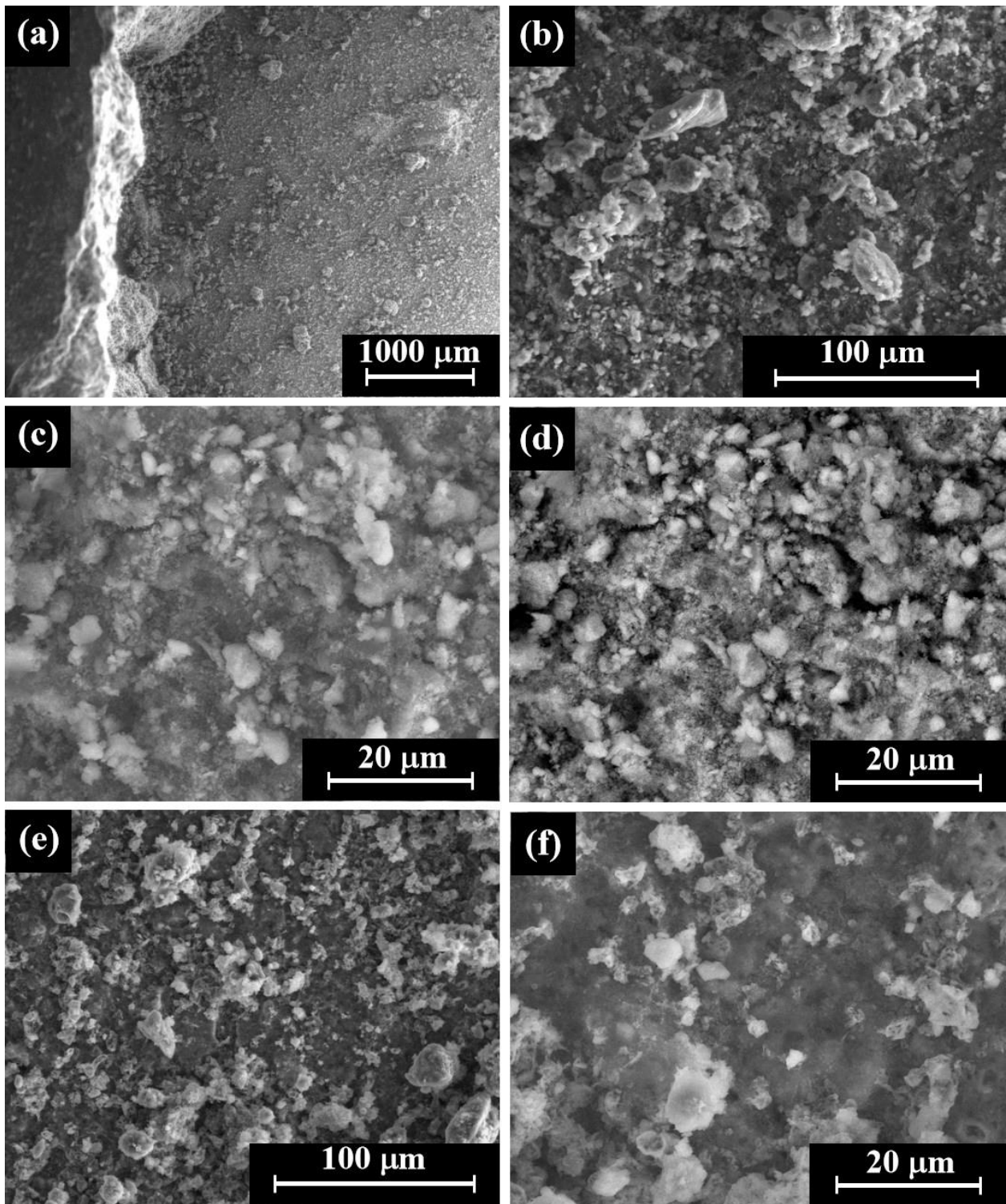


Figure 10. SEM images of the plaster (Sample no. 10, P-section): (a) general view of the upper (left side of image) and lower (right side of image) plaster layers; (b) view of the upper plaster layer; (c)–(d) higher magnification of the upper layer (SE and BSE modes, respectively); (e) view of the lower plaster layer (SE mode); and (f) higher magnification of the lower layer (SE Mode). A crystalline microstructure was observed in both layers, with large grains of 2–8 μm , as well as smaller crystalline grains of 200–600 nm in size.

Table 3. SEM-EDS chemical analysis of the plaster, where SA represents the scanned area.

| Sample description | Composition weight percentage (wt%) | | | | | | | | | |
|--|-------------------------------------|----------|----------|-----------|----------|-----------|-----------|-----------|-----------|----------|
| | <u>Ca</u> | <u>O</u> | <u>C</u> | <u>Si</u> | <u>S</u> | <u>Fe</u> | <u>Al</u> | <u>Mg</u> | <u>Na</u> | <u>K</u> |
| Fine and smooth plaster, reference sample (Fig. 9a, P-section), SA: 500 μm \times 500 μm | 35.3 | 48.8 | 12.5 | 1.5 | 0.3 | 0.4 | 0.6 | 0.3 | 0.3 | - |
| Fine and smooth plaster, Sample no. 4 (P-section, SA: 150 μm \times 150 μm) | 33.0 | 51.5 | 13.7 | 0.9 | 0.4 | - | 0.2 | - | 0.3 | - |
| Fine and smooth plaster, Sample no. 4 (T-CS), near decoration, SA: 100 μm \times 100 μm | 28.2 | 49.6 | 8.4 | 0.9 | 12.3 | - | 0.3 | 0.3 | - | - |
| Plaster, embedded white particles, Sample no. 4 (T-CS, Fig. 8c), near decoration, SA: 100 μm \times 100 μm | 27.3 | 52.3 | - | 0.2 | 20.2 | - | - | - | - | - |
| Plaster, Sample no. 10, upper layer (P-section), SA: 200 μm \times 200 μm | 31.1 | 48.6 | 11.1 | 4.5 | 0.5 | 1.3 | 1.3 | 0.6 | 0.4 | 0.6 |
| Plaster, Sample no. 10, lower layer (P-section), SA: 200 μm \times 200 μm | 40.4 | 45.4 | 10.4 | 2.1 | 0.2 | - | 0.6 | 0.5 | 0.4 | - |
| Plaster, reference sample (Fig. 9b, P-section), SA: 500 μm \times 500 μm | 30.8 | 50.4 | 13.6 | 2.0 | 0.3 | 1.5 | 0.6 | 0.5 | - | 0.3 |
| Plaster, reference sample (Fig. 9d, P-section), SA: 150 μm \times 150 μm | 34.0 | 48.3 | 9.9 | 3.3 | 1.5 | 0.8 | 1.0 | 0.6 | 0.2 | 0.4 |
| Coarse substrate plaster, reference sample (Fig. 8f), SA: 200 μm \times 200 μm | 34.4 | 58.4 | - | 3.6 | 0.5 | 0.7 | 0.8 | 0.6 | 0.5 | 0.5 |

4.2. The red pigment

VT inspection of the red color revealed two types of red; the first one is dark red (Figs. 6d upper layer, 6i, 7a, 7c, and 11a upper layer) which contains many cracks (Fig. 11c), and the second one is a bright and less dense red (Figs. 6a–b, 6e, 6h, 6m, 7j). XRF analysis results revealed that the elemental composition of the dark and bright red color is similar, with an iron content of 3.1–4.4 wt% Fe for the dark red hue and 1.0–3.0 wt% Fe for the bright red hue (Table 4). The elements Ca, Si, S, Al, K, Ti and P were also detected in both red hues. Yet, higher concentrations of calcium

and sulfur were observed in the bright red and higher concentrations of iron were observed in the dark red color (Table 4), indicating that the dark red pigment layer is denser and thicker than the bright red pigment layer. Therefore, the bright red was most probably mixed with calcium carbonate and calcium sulphate dihydrate minerals (Table 1) in order to achieve a brighter appearance. The composition of the red pigment layer was 1.0–4.4 wt% Fe according to XRF analysis (Table 4); whereas the iron concentration in the plaster was only 0.5–2.0 Fe wt% (Table 2), identifying the red hue as red ochre pigment.

Table 4. XRF chemical analysis of the red pigment.

| Sample description | Composition weight percentage (wt%) | | | | | | | | |
|----------------------------------|-------------------------------------|-----------|----------|-----------|-----------|-----------|----------|-----------|----------|
| | <u>Ca</u> | <u>Si</u> | <u>S</u> | <u>Fe</u> | <u>Al</u> | <u>Cl</u> | <u>K</u> | <u>Ti</u> | <u>P</u> |
| Sample no. 1, bright red | 19.0 | 4.5 | 8.0 | 3.0 | 0.8 | 0.1 | 0.4 | 0.1 | 0.2 |
| Sample no. 2, bright red | 35.4 | 2.5 | 0.3 | 1.4 | 0.6 | - | 0.3 | - | 0.2 |
| Sample no. 4, dark red | 16.9 | 5.0 | 6.3 | 4.4 | 1.1 | 0.1 | 0.5 | 0.2 | 0.2 |
| Sample no. 5, bright red, area 1 | 33.6 | 3.3 | 0.8 | 1.8 | 0.7 | 0.1 | 0.3 | 0.1 | 0.2 |
| Sample no. 5, bright red, area 2 | 30.1 | 4.4 | 1.1 | 2.6 | 1.3 | 0.1 | 0.5 | 0.2 | 0.2 |
| Sample no. 5, bright red, area 3 | 29.8 | 4.4 | 1.1 | 2.5 | 1.3 | - | 0.5 | 0.2 | 0.2 |
| Sample no. 7, bright red | 25.9 | 4.8 | 6.7 | 1.0 | 0.7 | 0.1 | 0.4 | 0.1 | 0.2 |
| Sample no. 8, bright red, area 1 | 33.2 | 3.3 | 1.0 | 1.7 | 1.2 | 0.1 | 0.4 | 0.1 | 0.2 |
| Sample no. 8, bright red, area 2 | 31.6 | 2.9 | 0.9 | 1.3 | 0.8 | - | 0.3 | 0.1 | 0.3 |
| Sample no. 9, dark red | 30.8 | 3.3 | 0.5 | 3.1 | 1.8 | - | 0.3 | 0.2 | 0.2 |
| Sample no. 11, bright red | 21.1 | 4.2 | 9.8 | 1.4 | 0.8 | - | 0.4 | 0.2 | 0.2 |
| Sample no. 13, dark red | 28.0 | 3.5 | 1.3 | 3.8 | 1.9 | - | 0.4 | 0.2 | 0.2 |

SEM observation of the dark red painted surface (Fig. 11a) revealed that it contains many cracks and is brighter than the plaster that surrounds it (Fig. 11b–c,

according to BSE mode), and also brighter than the brown-gray painted areas (Fig. 11d–f). Higher SEM magnifications revealed that the dark and bright red

pigments were composed of larger crystals of 2–6 μm in size and smaller crystals of 200–1000 nm in size (Fig. 12). SEM-EDS analysis of the dark red pigment revealed that it is mostly composed of iron oxide, with a composition of 15.0–22.7 wt% Fe, 41.9–48.0 wt% O, 7.1–9.5 wt% C, 7.8–8.7 wt% Si, 7.1–8.1 wt% Ca, 2.5–3.1 wt% S, 5.0–5.8 wt% Al, and up to 1.2 wt% of the elements Mg, Na, Cl, K, Ti and P (Table 5), indicating that the dark red pigment is red ochre. SEM-

EDS analysis of the bright red pigment revealed a similar composition to the dark pigment, however, with less iron content (11.3–12.8 wt% Fe) and with higher calcium content (19.3–19.8 wt% Ca) (Table 5). The EDS results (Table 5) are in relatively good agreement with the XRF results (Table 4), yet, the iron content in the SEM-EDS results is much higher as expected from surface analysis.

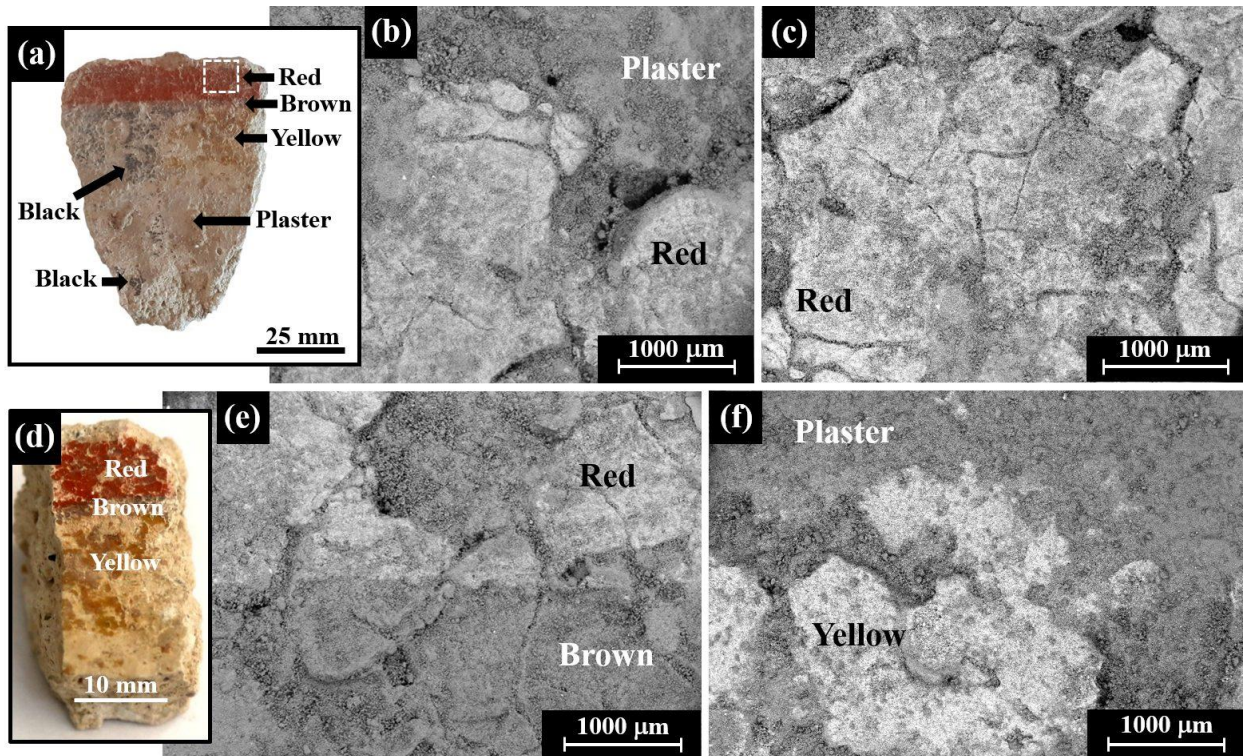


Figure 11. Images of the Sample no.4's decorated surface (P-section): (a) general view of the dark red, brown-gray, yellow and black pigments, as well as the areas of exposed plaster; and (b)–(c) SEM images of the dark red pigment (area inside the square in Fig. 11a, bright areas according BSE mode), showing the presence of many cracks surrounded by plaster (dark area according BSE mode), (d) a general view of the red, brown-gray and yellow pigments; (e) SEM image of the red pigment strip (upper bright area according to BSE mode) and the brown-gray strip (lower darker area); and (f) SEM image of the plaster and brown pigment strip (upper dark area) and the yellow pigment (lower bright zone according to BSE mode).

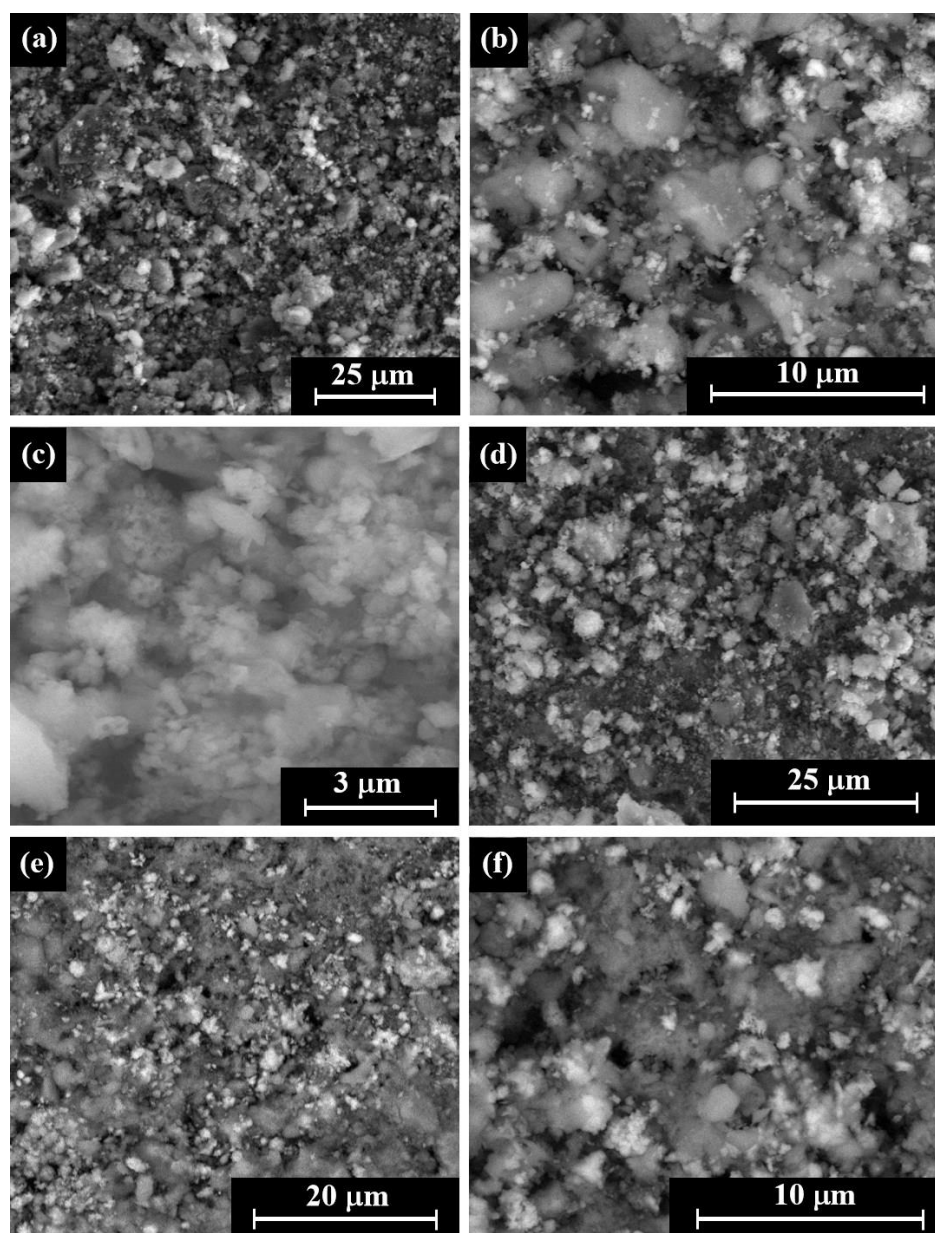


Figure 12. SEM images of the red pigment microstructure (P-section): (a) view of the dark red pigment surface (Sample no. 4, SE mode, area inside the square in Fig. 11a); (b)–(c) higher magnification of Fig. 12a (SE and BSE modes, respectively) showing larger crystals of 2–6 μm in size and smaller crystals of 200–800 nm in size; (d)–(e) general view of the bright red pigment surface (Sample no. 8, SE mode); and (f) higher magnification of Fig. 12e (Sample no. 8, BSE mode) showing larger crystals of 2–6 μm in size and smaller crystals of 200–1000 nm in size.

Table 5. SEM-EDS chemical analysis of the red pigment, where SA represents the scanned area.

| Sample description | Composition weight percentage (wt%) | | | | | | | | | | | | |
|--|-------------------------------------|------|-----|-----|-----|------|-----|-----|-----|-----|-----|-----|-----|
| | Ca | O | C | Si | S | Fe | Al | Mg | Na | Cl | K | P | Ti |
| Sample no. 4, dark red pigment (Fig. 12a), SA: 150 μm \times 150 μm | 8.1 | 41.9 | 7.9 | 8.7 | 3.1 | 22.7 | 5.0 | 0.8 | 0.5 | – | 0.9 | – | 0.4 |
| Sample no. 4, dark red pigment (Fig. 12b), SA: 25 μm \times 25 μm | 7.5 | 42.3 | 7.6 | 7.8 | 2.5 | 24.1 | 5.8 | 0.7 | 0.4 | 0.2 | 0.8 | – | 0.2 |
| Sample no. 4, dark red pigment (Fig. 12c), SA: 15 μm \times 15 μm | 7.1 | 48.0 | 9.5 | 8.4 | 2.6 | 15.0 | 5.5 | 0.5 | 0.5 | 0.3 | 1.2 | 0.2 | 0.2 |
| Sample no. 8, bright red (Fig. 12d), SA: 60 μm \times 60 μm | 19.3 | 47.6 | 7.8 | 5.2 | 0.5 | 12.8 | 5.2 | 0.4 | 0.5 | – | 0.5 | 0.2 | – |
| Sample no. 8, bright red (Fig. 12e), SA: 40 μm \times 40 μm | 19.8 | 48.0 | 8.3 | 5.4 | 0.3 | 11.3 | 5.1 | 0.7 | 0.2 | 0.2 | 0.7 | – | – |

4.3. The yellow pigment

VT inspection of the yellow color revealed it contains cracks (Fig. 7d, 7e, 7m, 7n), and it is surrounded by plaster material. XRF analysis of the yellow paint

revealed it contains 0.9–3.9 wt% Fe, as well as the presence of the elements Ca, Si, S, Al, Cl, K, P, and Ti (Table 6).

Table 6. XRF chemical analysis of the yellow pigment.

| Sample description | Composition weight percentage (wt%) | | | | | | | | |
|-------------------------------|-------------------------------------|-----|------|-----|-----|-----|-----|-----|-----|
| | Ca | Si | S | Fe | Al | Cl | K | Ti | P |
| Sample no. 4, yellow, area 1 | 21.2 | 4.3 | 6.0 | 3.3 | 0.7 | 0.2 | 0.5 | 0.1 | 0.2 |
| Sample no. 4, yellow, area 2 | 19.9 | 2.7 | 10.1 | 3.9 | 0.6 | 0.1 | 0.3 | - | 0.2 |
| Sample no. 11, yellow, area 1 | 19.7 | 3.2 | 9.9 | 3.0 | 0.7 | 0.1 | 0.3 | - | 0.2 |
| Sample no.11, yellow, area 2 | 23.4 | 4.5 | 8.5 | 0.9 | 1.0 | 0.1 | 0.5 | 0.2 | 0.3 |

SEM observation of the yellow painted surface revealed that it is much brighter than the brown pigment (Fig. 11d–f, BSE mode). Higher SEM magnification revealed larger crystals of 2–6 μm in size and smaller crystals of 300–1000 nm in size (Figs. 13 and 14). SEM-EDS analysis of the yellow pigment revealed it was mostly composed of iron oxide, with a composition of 22.8–26.1 wt% Fe, 42.5–45.0 wt% O,

7.5–11.5 wt% C, 7.0–10.8 wt% Ca, 2.0–8.3 wt% Si, 0.4–5.3 wt% Al, and up to 1.6 wt% of the elements Mg, Na, Cl, K, Ti, P and Pb (Table 7). The EDS analysis results (Table 7) are in relatively good agreement with the XRF results (Table 6), yet, the calcium content is much lower and the iron content much higher according to the SEM-EDS results, as expected.

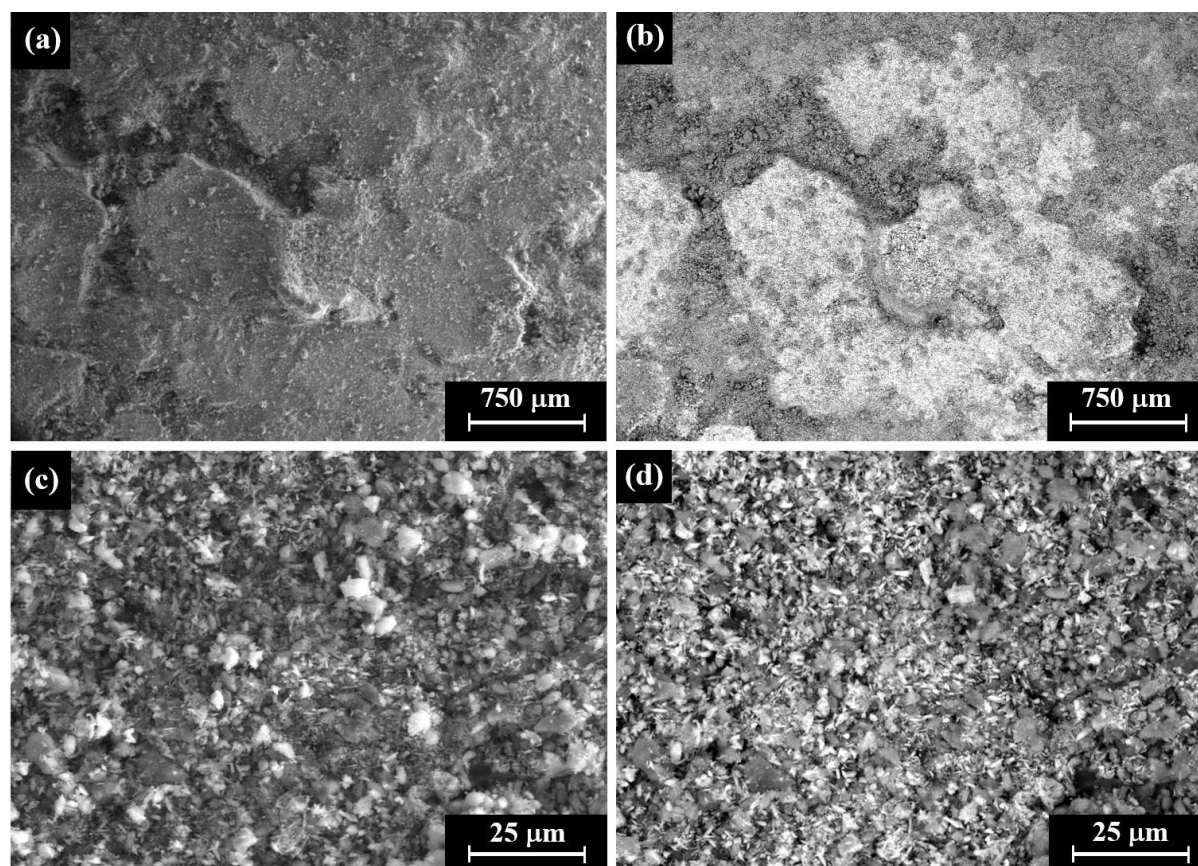


Figure 13. SEM images of the yellow pigment (Sample no. 4, P-section): (a)–(b) general view of the surface (SE and BSE modes, respectively); and (c)–(d) higher magnification of Fig. 13a (SE and BSE modes, respectively), showing large crystals of 2–5 μm in size and small crystals of 500–1000 nm in size.

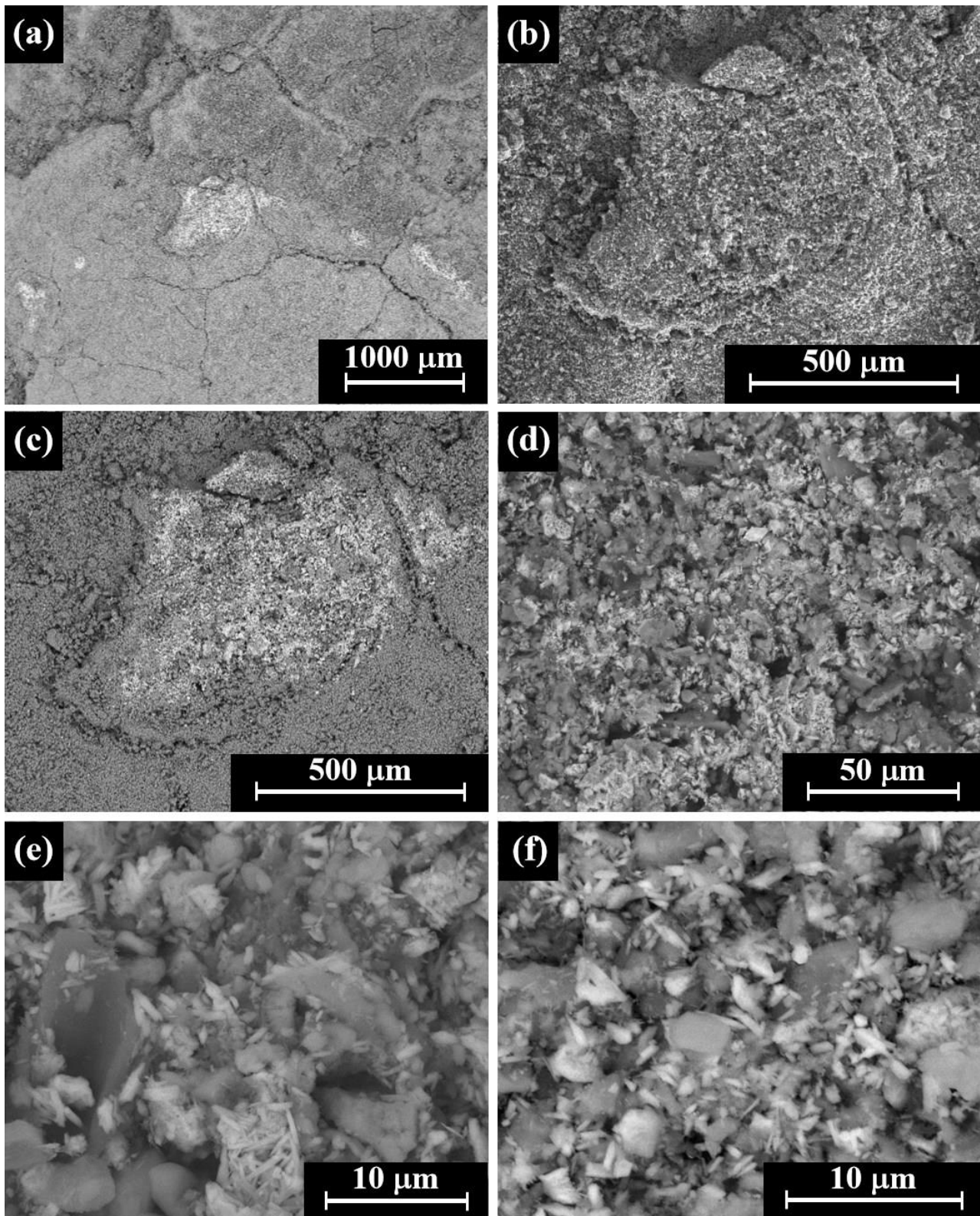


Figure 14. SEM images of the yellow pigment microstructure (Sample no. 4, P-section): (a) general view of the yellow pigment (bright area according to BSE mode) surrounded by plaster material (darker material); (b)–(c) higher magnification of the yellow pigment in Fig. 14a (SE and BSE modes, respectively); (d) higher magnification of Fig. 14c, showing crystalline microstructure; (e)–(f) higher magnification of two areas in Fig. 14d (SE and BSE modes, respectively), showing large crystals of 3–6 μm in size and small crystals of 300–1000 nm in size.

Table 7. SEM-EDS chemical analysis of the yellow pigment, where SA represents the scanned area.

| Sample description | Composition weight percentage (wt%) | | | | | | | | | | | |
|---|-------------------------------------|----------|----------|-----------|----------|-----------|-----------|-----------|-----------|-----------|----------|-----------------|
| | <u>Ca</u> | <u>O</u> | <u>C</u> | <u>Si</u> | <u>S</u> | <u>Fe</u> | <u>Al</u> | <u>Mg</u> | <u>Na</u> | <u>Cl</u> | <u>K</u> | <u>Other</u> |
| Sample no. 4, yellow pigment (Fig. 14c, inside the bright area), SA: 250 μm \times 250 μm | 10.8 | 42.5 | 11.5 | 2.0 | 5.4 | 24.2 | 0.4 | 0.5 | 0.3 | 0.3 | 0.3 | 1.6 Pb 0.2 P |
| Sample no. 4, yellow pigment (Fig. 14d), SA: 150 μm \times 150 μm | 10.5 | 45.0 | 8.6 | 3.4 | 7.5 | 26.1 | 1.0 | 0.7 | 0.4 | 0.3 | - | - |
| Sample no. 4, yellow pigment (Fig. 14f), SA: 25 μm \times 25 μm | 7.0 | 43.2 | 7.5 | 8.3 | 2.8 | 22.8 | 5.3 | 0.8 | 0.5 | 0.3 | 0.8 | 0.4 Ti 0.3 P |

4.4. The brown-gray pigment

VT inspection of the brown-gray color revealed a quite uniform surface (Figs. 6f, 7g), yet, areas with red tone were also observed, for example, the red line in

Sample no. 6 (Fig. 7h). XRF analysis of the brown-gray paint (Table 8) revealed a composition almost identical to the composition of the coarse and fine plaster layers (Table 2), with an iron content of 0.5–1.6 wt% Fe (Table 8).

Table 8. XRF chemical analysis of the brown-gray pigment.

| Sample description | Composition weight percentage (wt%) | | | | | | | | | |
|---|-------------------------------------|-----------|----------|-----------|-----------|-----------|----------|-----------|----------|--|
| | <u>Ca</u> | <u>Si</u> | <u>S</u> | <u>Fe</u> | <u>Al</u> | <u>Cl</u> | <u>K</u> | <u>Ti</u> | <u>P</u> | |
| Sample no. 14, brown-gray (higher area) | 29.5 | 5.5 | 2.9 | 1.6 | 0.9 | 0.1 | 0.6 | 0.2 | 0.3 | |
| Sample no. 14, brown-gray (lower area) | 33.5 | 3.6 | 2.9 | 0.9 | - | 0.1 | 0.4 | 0.1 | 0.2 | |
| Sample no. 15, brown-gray | 20.7 | 2.5 | 8.3 | 0.5 | - | - | 0.3 | 0.1 | 0.3 | |
| Sample no. 16, brown-gray, area 1 | 24.1 | 4.0 | 4.9 | 1.0 | 0.6 | 0.1 | 0.5 | 0.2 | 0.4 | |
| Sample no. 16, brown-gray, area 2 | 24.0 | 4.4 | 7.6 | 0.9 | 0.4 | 0.1 | 0.5 | 0.2 | 0.2 | |

SEM observation of the brown-gray pigment revealed both larger crystals of 2–6 μm in size and smaller crystals of 200–800 nm in size (Fig. 15). SEM-EDS analysis of the brown-gray pigment revealed a composition of 18.1–21.9 wt% Ca, 48.3–52.1 wt% O, 9.9–11.2 wt% C, 3.1–9.8 wt% Si, 1.0–10.8 wt% S, 2.3–3.1 wt% Fe, 1.4–3.6 wt% Al, and up to 1.6 wt% of the elements Mg, Na, Cl, K and P (Table 9). The EDS results (Table 9) are in relatively good agreement with the XRF results (Table 8); yet, the iron content in the SEM-EDS results is higher. Moreover, according to the EDS results, the iron content in the brown-gray paint (Table 9) is much lower than the content in the red and yellow paints (Tables 5 and 7, respectively), but much higher than the iron content in the plaster (Table 3).

The XRD analysis results of the brown color layer painted on top of the plaster material (Sample no. 6)

revealed that the main crystalline phase is calcium carbonate. Yet, picks of crystalline haematite, $\alpha\text{-Fe}_2\text{O}_3$ (red ochre pigment), goethite, $\alpha\text{-FeO(OH)}$ (yellow ochre pigment), and magnetite, Fe_3O_4 (common ingredient in brown ochre), as well as picks of graphite (carbon-based black pigments) were also detected (Fig. 16). In addition, picks of crystalline kaolinite [$\text{Al}_2\text{Si}_2\text{O}_5(\text{OH})_4$], quartz (SiO_2) and gypsum ($\text{CaSO}_4 \cdot 2\text{H}_2\text{O}$) minerals were also detected (Fig. 16). The results are with good agreement with the XRF and SEM-EDS analysis. The dominance of the calcium carbonate mineral in the brown color, as well as the quartz, gypsum and kaolinite may be explained according to the use of pigments mixed with ground powder of plaster material and according to the use of fresco method, resulting in a diffusion between the pigments and the plaster matrix base.

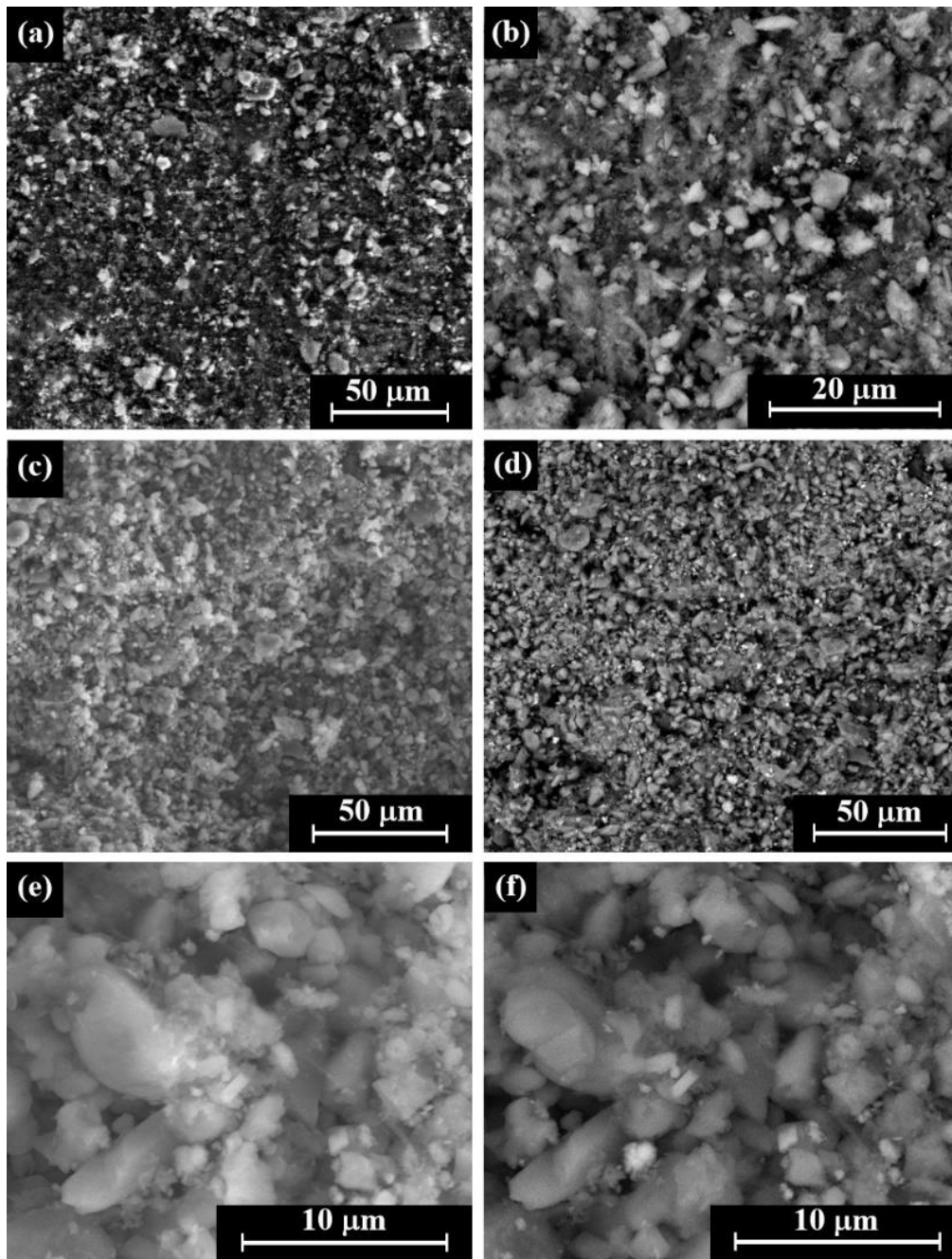


Figure 15. SEM images of the brown-gray pigment: (a) the external surface of Sample no. 6 (SE mode, P-section); (b) the crystalline microstructure, with large crystals of 2–5 μm in size and small crystals of 300–800 nm in size (Sample no. 6, BSE mode); (c)–(d) crystalline microstructure (Sample no. 4, SE and BSE modes, respectively); and (e)–(f) large crystals of 2–6 μm in size and small crystals of 200–800 nm in size (Sample no. 4, SE and BSE modes, respectively).

Table 9. SEM-EDS chemical analysis of the brown-gray pigment, where SA represents the scanned area.

| Sample description | Composition weight percentage (wt%) | | | | | | | | | | | |
|---|-------------------------------------|------|------|-----|------|-----|-----|-----|-----|-----|-----|-----|
| | Ca | O | C | Si | S | Fe | Al | Mg | Na | Cl | K | P |
| Sample no. 6, brown-gray (Fig. 15a), SA: 150 $\mu\text{m} \times 150 \mu\text{m}$ | 21.9 | 48.3 | 11.0 | 7.8 | 3.7 | 2.3 | 2.7 | 1.2 | 0.3 | 0.2 | 1.1 | 0.4 |
| Sample no. 6, brown-gray (Fig. 15a), SA: 50 $\mu\text{m} \times 50 \mu\text{m}$ | 20.4 | 48.6 | 9.9 | 9.8 | 1.1 | 3.1 | 3.6 | 1.6 | 0.4 | 0.3 | 1.2 | - |
| Sample no. 4, brown-gray hue (Fig. 15c), SA: 150 $\mu\text{m} \times 150 \mu\text{m}$ | 19.4 | 50.9 | 11.2 | 3.8 | 9.0 | 2.6 | 1.4 | 0.7 | 0.2 | 0.3 | 0.4 | 0.1 |
| Sample no. 4, brown-gray hue (Fig. 15e), SA: 25 $\mu\text{m} \times 25 \mu\text{m}$ | 18.1 | 52.1 | 10.9 | 3.1 | 10.8 | 2.5 | 1.4 | 0.5 | 0.3 | - | 0.3 | - |

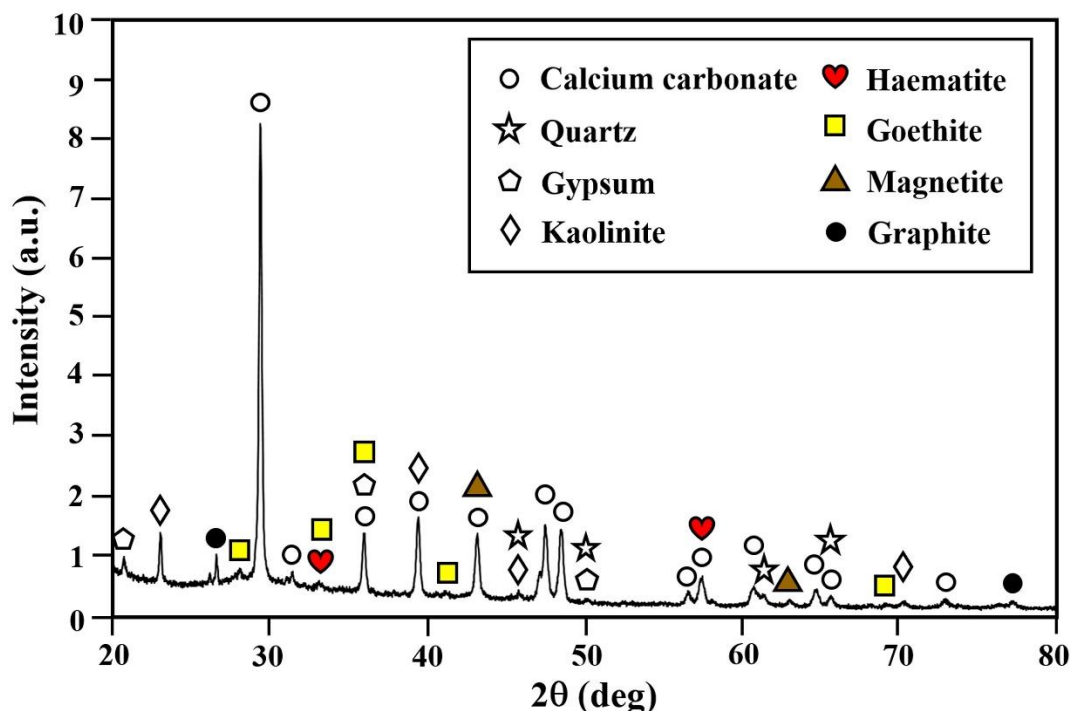


Figure 16. XRD analysis results of the brown paint on top of the plaster (Sample no. 6).

4.5. The black pigment

VT inspection of the black color revealed that it contains many cracks (Figs. 7f). XRF analysis of the black paint (Table 10) revealed a composition almost

identical to the composition of the plaster (Table 2), as well as of the brown-gray paint (Table 8), with iron content of 0.7–2.6 wt% Fe (Table 10).

Table 10. XRF chemical analysis of the black pigment.

| Sample description | Composition weight percentage (wt%) | | | | | | | | |
|-----------------------------|-------------------------------------|-----|------|-----|-----|-----|-----|-----|-----|
| | Ca | Si | S | Fe | Al | Cl | K | Ti | P |
| Sample no. 1, black, area 1 | 21.8 | 5.4 | 6.4 | 1.6 | 0.9 | 0.2 | 0.6 | 0.1 | 0.2 |
| Sample no. 1, black, area 2 | 20.9 | 4.2 | 8.8 | 1.7 | 0.6 | 0.2 | 0.4 | 0.1 | 0.2 |
| Sample no. 1, black, area 3 | 19.5 | 4.3 | 9.0 | 2.6 | 1.2 | 0.1 | 0.4 | 0.1 | 0.1 |
| Sample no. 4, black | 24.2 | 3.6 | 10.6 | 0.7 | 0.6 | 0.1 | 0.4 | 0.1 | 0.2 |
| Sample no. 7, black | 23.6 | 4.5 | 7.1 | 0.7 | 0.7 | 0.2 | 0.4 | 0.1 | 0.3 |

SEM observation of the black pigment revealed both larger crystals of 2–5 μm in size and smaller crystals of 600–1000 nm in size (Fig. 17). SEM-EDS analysis of the black pigment revealed a composition of 22.5–30.2 wt% Ca, 46.7–52.8 wt% O, 8.5–10.3 wt% C, 2.5–4.0 wt% Si, 7.5–8.1 wt% S, 0.8–1.4 wt% Fe, 0.9–1.7

wt% Al and up to 0.7 wt% of the elements Mg, Na, and K (Table 11). According to the EDS results, the iron content in the black paint (Table 11, 0.8–1.4 wt% Fe) is lower than the content in the brown-gray paints (Tables 9, 2.5–2.6 wt% Fe).

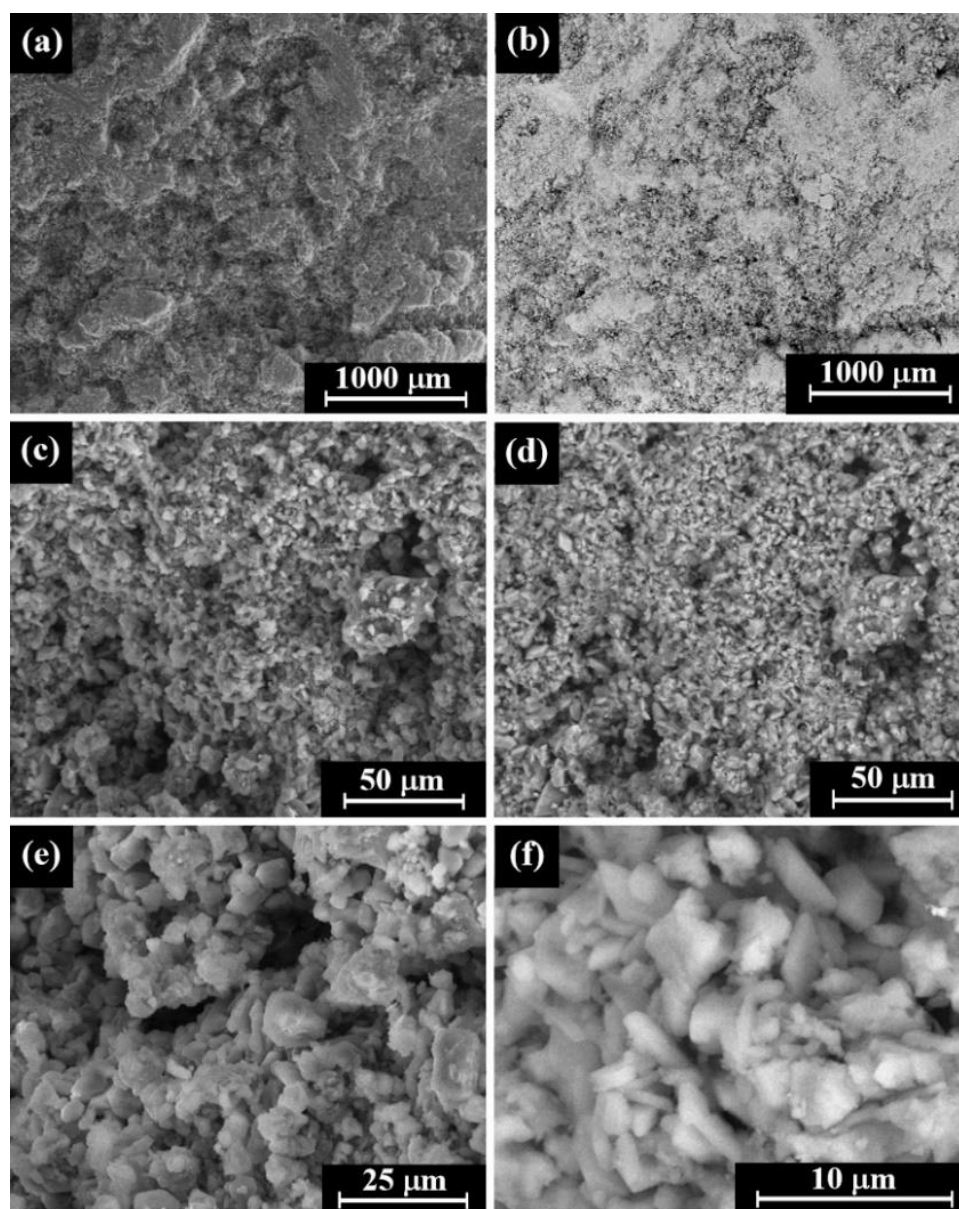


Figure 17. SEM images of the black pigment (Sample no. 4, P-section): (a) general view of the black pigment, showing a rough surface (SE mode); (b) general view (BSE mode); (c)–(d) crystalline microstructure (SE and BSE modes, respectively); (e)–(f) higher magnification of the crystalline microstructure, showing larger crystals of 2–5 μm in size and smaller crystals of 600–1000 nm.

Table 11. SEM-EDS chemical analysis of the black pigment, where SA represents the scanned area.

| Sample description | Composition weight percentage (wt%) | | | | | | | | | | |
|--|-------------------------------------|----------|----------|-----------|----------|-----------|-----------|-----------|-----------|-----------|----------|
| | <u>Ca</u> | <u>O</u> | <u>C</u> | <u>Si</u> | <u>S</u> | <u>Fe</u> | <u>Al</u> | <u>Mg</u> | <u>Na</u> | <u>Cl</u> | <u>K</u> |
| Sample no. 4, black pigment (Fig. 17a), SA: 800 μm \times 800 μm | 27.1 | 50.0 | 8.5 | 3.2 | 8.0 | 1.0 | 1.1 | 0.7 | - | - | - |
| Sample no. 4, black pigment (Fig. 17c), SA: 150 μm \times 150 μm | 30.2 | 46.7 | 10.3 | 2.5 | 7.5 | 0.8 | 0.9 | 0.5 | 0.2 | - | 0.4 |
| Sample no. 4, black pigment (Fig. 17e), SA: 50 μm \times 50 μm | 22.5 | 52.8 | 8.9 | 4.0 | 8.1 | 1.4 | 1.7 | 0.6 | - | - | - |

5. DISCUSSION

The plaster and pigments retrieved from the wall paintings of the Hellenistic Tell Izt̄abba site were

studied by a multidisciplinary approach in order to gain information concerning their composition, microstructure, the raw materials' origin, as well as the

technologies that were used to paint the walls. For example, VT and SEM-EDS observation of the T-CS of Sample no. 4 revealed the use of the fresco technique, with gradual changes between the painted layer and the plaster beneath it (Figs. 8d, 9c).

The plaster was made of calcium carbonate matrix with up to 2 mm embedded aggregates. For all examined samples, the plaster layer near the painting is finer and smoother than the back side of the plaster, which attests to a different type of plastering of the walls' inner and outer surfaces. SEM-EDS analysis results revealed that the main elements in the plaster were Ca, O, C, and Si (Table 3). Higher Si suggests improved resiliency to water. Based on VT, XRF and SEM-EDS analyses, the plaster of all samples was similar in composition and contained mostly calcium carbonate (calcite, CaCO_3), with silica presence (Tables 2 and 3), indicating that it was made of a lime binder (matrix) and embedded aggregate minerals, such as quartz sand, kaolinite, and potassium feldspar, as expected from the literature review (Apostolaki et al., 2006, p. 731; Klempan et al., 2017, p. 1078; Mateos et al., 2018, p. 22). SEM observation of the fine plaster external surface revealed relatively a uniform exterior (Figs. 9–10). According to XRF and analysis results,

the Si content was higher in the substrate plaster than in the fine plaster cover (Table 2). According to the SEM-EDS analysis results, the fine plaster contains slightly more calcium and somewhat less silicone compared to the coarse plaster (Table 3); this may be explained according to more embedded sand particles in the rough and coarse plaster compared to the fine plaster. The XRF analysis and the EDS analysis results of the studied plaster are in good agreement (Table 2 and 3, respectively). Based on the SEM-EDS analysis (Table 3), the plaster substrate layer consists of calcite crystals with grains of 2–8 μm in size (Fig. 8f–g, T-CS), whereas the top plaster layer consists of coarser grains, with grains of 1–8 μm in size, and finer grains, 0.2–0.7 μm in size (Figs. 9 and 10, Table 12, P-section). These results are in agreement with the published literature; for example, Duran and his colleagues studied Roman and Arabic wall paintings retrieved from the Patio De Banderas, located in the Reales Alcazares' Palace of Seville, Spain, and found that the calcite grains in the plaster were 1–3 μm in size. Yet, according to Duran and his colleagues, the observed red haematite grains and yellow goethite grains were less than 0.5 μm in size (Duran et al., 2011, p. 2373).

Table 12. The observed grain size of the plaster and pigments (according to SEM observation).

| Color | Sample no. | Larger crystals (μm) | Smaller crystals (μm) |
|------------------------------------|------------------|-----------------------------------|------------------------------------|
| Coarse plaster surface (Fig. 8f–g) | Reference sample | 2–8 | – |
| Fine plaster (Fig. 9a–b) | Reference sample | 1–5 | 0.2–0.6 |
| Fine plaster (Fig. 9e–f) | Sample no. 4 | 1–4 | 0.3–0.7 |
| Fine plaster (Fig. 10) | Sample no. 10 | 2–8 | 0.2–0.6 |
| Dark red (Fig. 12a–c) | Sample no. 4 | 2–6 | 0.2–0.8 |
| Bright red (Fig. 12d–f) | Sample no. 8 | 2–6 | 0.2–1.0 |
| Yellow (Fig. 13) | Sample no. 4 | 2–5 | 0.5–1.0 |
| Yellow (Fig. 14) | Sample no. 4 | 3–6 | 0.3–1.0 |
| Brown-gray (Fig. 15a–b) | Sample no. 6 | 2–5 | 0.3–0.8 |
| Brown-gray (Fig. 15c–f) | Sample no. 4 | 2–6 | 0.2–0.8 |
| Black (Fig. 17) | Sample no. 4 | 2–5 | 0.6–1.0 |

Preliminary identification of the pigments was done based on the VT inspection combined with a comparison of the current pigment catalogue (Fig. 7) and the existing literature. VT inspection of the red color and comparison of the pigment catalogue (Fig. 7a, 7c, 7j) to the literature show that the red hue is probably related to red ochre (Aquilina et al., 2012, p. 230; Balandier et al., 2017, p. 334; Gajić-Kvaščev et al., 2012; Marketou et al., 2019; Mateos et al., 2018, pp. 16–17; Miriello et al., 2018; Roebroeks et al., 2012, p. 1890; Sajó et al., 2015, p. 5). Comparison of the yellow paint (Fig. 7d, 7e, 7m, 7n, pigment catalogue) to the literature shows that the yellow tone is probably related to yellow ochre (Aquilina et al., 2012, p. 230; Balandier et al., 2017, p. 334; Marketou et al., 2019; Mateos et al., 2018, pp. 16–17; Miriello et al., 2018). VT and catalogue observation of the black paint (Fig. 7f, pigment

catalogue) revealed that the black hue is probably related to carbon-based black pigments (Miriello et al., 2018; Tomasini et al., 2012, p. 36).

The XRF analysis results of the red color revealed it was composed of iron (1.3–4.4 wt% Fe), Ca, Si, S, Al, Cl, K, P, and Ti (Table 4). The XRF analysis results of the red color revealed an almost similar composition of the plaster. The similar results may be explained according to the fact that the XRF method is a bulk analysis technique; therefore, the information depends on the depth of penetration of the XRF instrument, which may range between $\sim 1 \mu\text{m}$ up to few centimeters, depending on the examined elements. Yet, according to the XRF results the amount of iron in the red paint (Table 4) is significantly higher than in the plaster materials (with 0.5–3.4 wt% Fe, Table 2). The composition received from the XRF analysis of the dark and bright red color was similar; yet, a higher

concentration of Ca was detected in the bright red color and a higher concentration of Fe was noticed in the dark red color, indicating that the dark red pigment layer was denser and thicker than the bright red pigment layer (Table 4). For a comparison, the XRF analysis results of the red ochre pigment identified in the terra rossa soil near the Neolithic site of Kfar HaHoresh, Israel was composed of the elements iron (4.6 wt% Fe), Ca, Si, S, Al, Cl, K, P, Mn, and Mg (Tsatskin and Gendler, 2016, p. 284). SEM observation of the present dark red color revealed many cracks. Larger crystals of 2–6 μm in size and smaller crystals of 200–1000 nm in size were observed by SEM on the surface of the dark and bright red hues (Fig. 12). SEM-EDS analysis of the dark and bright red pigments revealed that both are composed of iron oxide. The dark red hue contained 15.0–22.7 wt% Fe, and the bright red hue contained 11.3–12.8 wt% Fe; yet, other elements, including O, C, Si, Ca, S, Al, Mg, Na, Cl, K, Ti and P, were also identified in the dark and bright red hue (Table 5), as typical of red ochre pigment. The current EDS results of the red pigments are in good agreement with the XRF results (Table 5 and Table 4, respectively); yet, the iron concentration in the SEM-EDS results is much higher, as expected from the surface elemental technique. The EDS analysis results (Table 5) show a larger amount of iron in the red paint than in the plaster material (Table 3). The XRF and SEM-EDS current results are also in good agreement with the literature. For a comparison, PIXE analysis results of red colored samples, which were excavated from the Vinča Neolithic period culture archaeological site (Serbia) and identified as red ochre pigment, revealed a composition of 4.7–4.9 wt% Fe, 27.0–30.0 wt% Si, 2.0–7.0 wt% Ca, 1.3–1.9 wt% K as major elements (Gajić-Kvaščev *et al.*, 2012, p. 1032). Based on current VT examination, XRF and SEM-EDS chemical analyses of the red hue and the observed microstructure, the red color retrieved from the decorated walls of Tell Izṭabba was identified as red ochre pigment.

The XRF analysis results of the yellow color revealed it was composed of iron (0.9–3.9 wt% Fe), Ca, Si, S, Al, Cl, K, P, and Ti (Table 6), which is a much higher iron content than the amount detected in the plaster (Table 2) and almost identical to the XRF analysis of the red color (Tables 4). SEM observation of the yellow pigment revealed that it is similar to the red pigment brightness; yet, the yellow pigment is much brighter than the brown pigment (Fig. 11, BSE mode). Larger crystals of 2–6 μm in size and smaller crystals of 300–1000 nm in size were observed in the yellow pigment (Figs. 13 and 14). SEM-EDS analysis of the yellow pigment revealed it was mostly composed of iron oxide (goethite), with 22.8–26.1 wt% Fe and 42.5–45.0 wt% O (Table 7). Moreover, according

to SEM-EDS analysis, the amount of sulfur in the yellow pigment (2.8–7.5 wt% S) is higher than in the red pigment (0.3–3.1 wt% S) (Tables 7 and 5, respectively). Therefore, it is possible that potassium jarosite, $\text{KFe}_3(\text{SO}_4)_2(\text{OH})_6$, was also used in addition to the iron oxide in order to produce the yellow color. The XRF and SEM-EDS analysis results of the yellow color (Tables 6 and 7, respectively) are in relatively good agreement, but the calcium content is much lower and the iron content much higher according to the SEM-EDS results (Table 7), as expected from a surface elemental technique. Based on the VT examination of the hue, XRF and SEM-EDS chemical analyses, and the observed microstructure, the yellow paint was identified as yellow ochre pigment.

XRF analysis of the brown-gray paint (Table 8) revealed a composition almost identical to the plaster composition (Table 2), with an iron content of 0.5–1.6 wt% Fe for the brown-gray paint (Table 8). SEM observation of brown-gray pigment show both larger crystals of 2–6 μm in size and smaller crystals of 200–1000 nm in size (Fig. 15). SEM-EDS analysis of the brown-gray pigment revealed the presence of 2.3–3.1 wt% Fe and 1.1–10.8 wt% S (Table 9). The EDS analysis results are in good agreement with the XRF analysis results (Tables 9 and 8, respectively); nevertheless, the iron amount in the SEM-EDS results is higher than in the XRF results, as expected. In addition, according to the EDS results, the iron content in the brown-gray paint (Table 9) is much lower than its content in the red and yellow paints (Tables 5 and 7, respectively), but much higher than the iron content in the plaster (Table 3). Although the main detected phase of the brown-gray paint was calcium carbonate according to the XRD analysis results, other crystalline phases were also detected, such as haematite, goethite, and magnetite minerals, as well as graphite phase (Fig. 16). In the Hellenistic, and Roman periods it was a common practice to mix different pigments in order to achieve a desired color shade (Barone *et al.*, 2018, p. 390). Therefore, based on VT examination, XRF analysis, SEM observation with both SE and BSE modes, SEM-EDS analysis, and XRD analysis, the brown-gray paint was a mixture of red ochre, yellow ochre, magnetite mineral and carbon black-based pigments mixed with fine ground plaster powder (mostly calcium carbonate). This conclusion is in good agreement with the literature (Barone *et al.*, 2018; Iordanidis *et al.*, 2014; Klempan *et al.*, 2017; Marketou *et al.*, 2019; Piovesan *et al.*, 2016).

XRF analysis of the black paint (Table 10) revealed a composition almost identical to the plaster as well as to the brown-gray paint (Tables 2 and 8, respectively), with an iron content of 0.7–2.6 wt% Fe (Table 10). SEM observation revealed larger crystals of 2–5 μm in size and smaller crystals of 600–1000 nm in size

(Fig. 17). According to the SEM-EDS analysis results, the iron content in the black paint (0.8–1.4 wt% Fe, Table 11) is lower than the content in the brown-gray paints (2.3–3.1 wt% Fe, Table 9). The use of carbon-based black pigment for wall painting was common in the Land of Israel during antiquity. For instance, Piovesan and his colleagues (2016) concluded that the black color from the walls of the Migdal (Magdala) synagogue and a Roman villa at Lod, Israel were made with carbon-based black at both Roman Empire period sites (Piovesan et al., 2016, p. 441). Even though carbon content is not quantifiable by SEM-EDS analysis on graphite-coated samples, the absence of further elements attributed to other black pigments, such as bone black, which contains phosphorus, and vegetable bone black, which contains potassium, indicates the use of carbon (coal) black or charcoal black pigments (Duran et al., 2011, p. 2375; Piovesan et al., 2016, p. 441). Therefore, based on the VT examination, XRF, SEM BSE mode observation, and SEM-EDS chemical analyses, the black paint was identified as carbon-based black pigment.

Based on the current research analysis results, the coarse plaster and fine plaster were identified as mostly made of calcium carbonate, CaCO_3 , which was one of the most common white pigments (lime white, Table 1) used in murals during antiquity. Yet, the embedded white particles, such as the one observed in Fig. 8c, were made of a calcium sulphate mineral. Tufa stone, which is a type of limestone, is one of the main rocks in the area of Beth She'an Valley. Gypsum ($\text{CaSO}_4 \cdot 2\text{H}_2\text{O}$) was also a common white pigment during antiquity (white gypsum, Table 1). In the region of the Beth She'an Valley there are gypsum deposits that were used since the beginning of the second millennium BCE as building materials (Maier, 2020, p. 6). The composition of the plaster found in Tell Iztabba is similar to the plaster materials found in other Hellenistic period sites in Israel (Segal and Porat, 1997). Therefore, the raw materials used for the production of the plaster were probably brought from the near neighborhood and, based on the chemical analyses results, both lime and gypsum may have been used (Tables 2 and 3). The red paint was identified as red ochre pigment (rich in haematite, $\alpha\text{-Fe}_2\text{O}_3$, mixed with plaster material); the yellow pigment was identified as yellow ochre pigment [mainly Goethite, $\alpha\text{-FeO(OH)}$] mixed with plaster; the brown paint was identified as a mixture of red ochre, yellow ochre and carbon black-based pigments mixed with plaster; and the black paint was identified as carbon black-based pigment mixed with plaster. The coarse plaster includes crystals with grain of 2–8 μm in size. The fine plaster contains coarser grains, 1–8 μm in size, and finer grains, 0.2–0.7 μm in size. The pigments also include coarser grains, 2–6 μm in size, and finer grains,

0.2–1.0 μm in size (Table 12). Therefore, the pigments were perhaps intentionally mixed with calcium carbonate or this may be the result of the use of the fresco technique. The red and yellow pigments observed by SEM, BSE mode as bright areas are observed because they are heavier materials than the calcite, quartz, and graphite phases; yet, the calcium carbonate matrix and the brown-gray and black pigments were observed by BSE mode as dark gray areas because of their lower density. The density of haematite (red) is 5.30 g/cm^3 ; the density of goethite (yellow) is 3.80 g/cm^3 ; the density of magnetite is 5.17 g/cm^3 (dark brown, gray to black); the density of calcium carbonate (white) is 2.71 g/cm^3 ; the density of quartz, SiO_2 , is 2.65 g/cm^3 ; and the density of the graphite carbon (black) is 2.26 g/cm^3 (Westlake et al., 2012). White calcium carbonate, red ochre, yellow ochre pigment, and carbon black-based pigments are ubiquitous materials in the Mediterranean region, including Israel. For example, Piovesan and his colleagues examined wall painting pigments of Roman period sites (Migdal and Lod, Israel), and concluded that red, yellow and brown were most likely regionally supplied. White calcium carbonate, red ochre, yellow ochre, and black carbon-based pigments were observed at other sites from the Hellenistic period in Israel, such as 'Akko (Ptolemais), Jericho and Maresha (Marisa) (Kakoulli, 2002, p. 62; Segal and Porat, 1997), and Tel Anafa (Kidd, 1999). Therefore, it is most reasonable that the pigments examined in the current study were made of raw materials from the site environs.

Based on the current research results, a four step methodology is suggested in order to study plaster and pigments from archaeological decorated walls. (1) The literature review should include archaeological information as well as mineralogical and technological aspects. (2) The examination should start with VT examination. In addition, it is mostly recommended to build a color catalogue (Fig. 7) that would help to compare the pigments to those that appear in the literature. Such a catalogue may be built by using a camera equipped with special lenses and creating a lighting environment that simulates daylight, and/or by using stereoscopic microscope, and/or by multifocal microscope (Ashkenazi and Cvikel, 2020). (3) The chemical analysis for plaster and pigment identification should be done by at least two of the following methods: XRF, SEM P-section and T-CS observations of the samples with both SE and BSE modes combined with EDS analysis, XRD analysis, Raman spectroscopy, and FTIR spectroscopy (Amadori et al., 2021; Crupi et al., 2018, p. 423; Fostiridou et al., 2016, p. 453; Gil-Torrano et al., 2019, p. 5; Guirdzhiiska et al., 2017, p. 431; Gutman et al., 2016, p. 194; Holakoei et al., 2016; Linn, 2017, p. 776; Liritzis et al., 2020; Marcaida et al., 2017; Marketou et al., 2019; Mateos et al., 2018;

Siddall, 2018; Taglieri et al., 2019, p. 158). In addition, other methods may be also used, including: Py-GC-MS, PIXE analysis, NAA, ICP-AES, inductively coupled mass spectrometry ICP-MS, LA-ICP-MS, XPS, HRSEM, and TEM (Arizzi and Cultrone, 2021; Dayet, 2021; Di Stefano and Fuchs, 2011; Garilli et al., 2020; Klempner et al., 2017; Liritzis et al., 2020; Piovesan et al., 2016; Tsatskin and Gendler, 2016). (4) The discussion and conclusions should be based on a comparison of the obtained results with those that appear in the literature, including taking into account both the date of the wall paintings and the geographical location of the archaeological site.

6. CONCLUSIONS

Fragments of Hellenistic wall paintings retrieved from Tell Iztabba were studied using a multidisciplinary approach in order to study the chemical composition, microstructure, technologies used and, if possible, the origin of the plaster and pigment raw materials. Based on current research results, the plasters

were composed of calcium carbonate matrix with embedded aggregates, including a calcium sulphate mineral and sand particles. The red and yellow paints were identified as red and yellow ochre pigments, respectively, the brown paint was a mixture of red ochre, yellow ochre, magnetite mineral and carbon black-based pigments, and the black paint was carbon black-based pigment, probably graphite black; all were mixed with fine plaster powder. The plaster and pigments were most probably locally supplied. The Tell Iztabba pigments are similar to pigments retrieved from other Hellenistic period sites in Israel, underlining that the settlers of the Seleucid town participated in local technical knowledge and regional supply chains, as we have observed regarding their adaptation to local agricultural practices (Orendi et al., 2021). Adopting the “first Pompeian style”/“Masonry Style” on the walls of their dwellings, likely as an Hellenized token of their shared identity with other such Hellenistic centers, may attest to the cosmopolitan character of the site and its settlers.

AUTHOR CONTRIBUTION

A.L. and O.T. defined the research aims and were in charge of the project administration, resources and funding acquisition; O.T. was in charge of the supervision; D.A. and O.T. defined the structure of the publication and were in charge of the conceptualization and original draft preparation; R.S. was in charge of the initial literature review; A.L. and O.T. wrote the introduction; D.A. wrote the technological background, contributed to the development of the experimental methodology and was in charge of the formal analysis; R.S. was in charge of the XRF analysis; D.A. was in charge of the catalogue of the plaster and pigments and of the SEM-EDS and XRD analyses. All authors discussed the results, wrote the discussion and conclusions, and contributed substantially to the work reported. All authors have read and agreed to the published version of the manuscript.

ACKNOWLEDGEMENTS

The excavations form part of a German-Israeli research project ‘Tell Iztabba (Nysa-Scythopolis): High-resolution Hellenistic Settlement Archaeology and the Reassessment of the Formation of the Decapolis, mainly funded by the German-Israeli Foundation for Scientific Research and Development (GIF Regular Program [grant I-150-108.7-2017]), to which we are grateful. The project was licensed by the Israel Antiquities Authority (G-70/2019; G-17/2020) and the Israel Nature and Parks Authority (A-014/19; A-020/20). We thank Tomer Reuveni of the Wolfson Applied Materials Research Center, Tel Aviv University for his valuable SEM technical assistance.

REFERENCES

- Aquila, E., Barone, G., Crupi, V., Longo, F., Majolino, D., Mazzoleni, P. and Venuti, V. (2012) Spectroscopic analyses of Hellenistic painted plasters from 2nd century BC, Sicily (South Italy). *Journal of Cultural Heritage*, Vol. 13, No. 2, pp. 229–233.
- Ali, M. F. and Elrahim, A. M. (2021). Analytical study of the blue pigment used in Ottoman house mural paintings, Cairo, Egypt. *Scientific Culture*, Vol. 7, No. 3, pp. 41–51. DOI: 10.5281/zenodo.4916497.
- Ali, M. F. and Youssef, M. M. (2020). An analytical study of a mural with colorful geometric decoration, Coptic Museum, Cairo, Egypt: a case study. *Scientific Culture*, Vol. 6, No. 3, pp. 37–52. DOI: 10.5281/zenodo.3956807.
- Amadori, M. L., Barcelli, S., Poldi, G., Ferrucci, F., Andreotti, A., Baraldi, P. and Colombini, M. P. (2015) Invasive and non-invasive analyses for knowledge and conservation of Roman wall paintings of the Villa of the Papyri in Herculaneum. *Microchemical Journal*, Vol. 118, pp. 183–192.

- Amadori, M. L., Vagnini, M., Vivani, R., Anselmi, C., Chaverdi, A. A., Callieri, P., Matin, E. and Mengacci, V. (2021) Advances in characterization of colourful residues unearthed in Persepolis West craft zone using microscopic and spectroscopic techniques. *Microchemical Journal*, Vol. 167, p. 106304.
- Apostolaki, C., Perdikatsis, V., Repuskou, E., Brecolouaki, H., and Lepinski, S. (2006) Analysis of Roman wall paintings from ancient Corinth/Greece. *The 2nd International Conference on Advances in Mineral Resources Management and Environmental Geotechnology*, Hania, Greece, pp. 729–734.
- Arizzi, A. and Cultrone, G. (2021) Mortars and plasters – how to characterise hydraulic mortars. *Archaeological and Anthropological Sciences*, Vol. 13, No. 9, pp. 1–22.
- Asderaki-Tzoumerkioti, E. L. and Doulgeri-Intzesiloglou, A. R. (2010) Hellenistic terracotta figurines from Pherai: tin foil detection and pigment identification. *Restaurierung und Archäologie*, Vol. 3, pp. 151–161.
- Ashkenazi, D. and Cvikel, D. (2020) A journey into the microstructure: Using a multifocal 3D digital light microscope to study archaeological artefacts retrieved from shipwrecks. *Digital Applications in Archaeology and Cultural Heritage*, Vol. 16, p. e00129.
- Balandier, C., Joliot, C., Menager, M., Vouve, F. and Vieillescazes, C. (2017) Chemical analyses of Roman wall paintings recently found in Paphos, Cyprus: The complementarity of archaeological and chemical studies. *Journal of Archaeological Science: Reports*, Vol. 14, pp. 332–339.
- Barone, G., Mazzoleni, P., Cecchini, A. and Russo, A. (2018) In situ Raman and pXRF spectroscopic study on the wall paintings of Etruscan Tarquinia tombs. *Dyes and Pigments*, Vol. 150, pp. 390–403.
- Birney, K. (2017) Phoenician bathing in the Hellenistic East: Ashkelon and beyond. *Bulletin of the American Schools of Oriental Research*, Vol. 378, pp. 203–222.
- Buzgar, N., Apopei, A. I. and Buzatu, A. (2013) Characterization and source of Cucuteni black pigment (Romania): vibrational spectrometry and XRD study. *Journal of Archaeological Science*, Vol. 40, No. 4, pp. 2128–2135.
- Cerrato, E. J., Cosano, D., Esquivel, D., Jiménez-Sanchidrián, C. and Ruiz, J. R. (2021) Spectroscopic analysis of pigments in a wall painting from a High Roman Empire building in Córdoba (Spain) and identification of the application technique. *Microchemical Journal*, Vol. 168, p. 106444. <https://doi.org/10.1016/j.microc.2021.106444>.
- Coccatto, A., Caggiani, M. C., Occhipinti, R., Mazzoleni, P., D'Alessio, A., Russo, A. and Barone, G. (2021) The irreplaceable contribution of cross-sections investigation: Painted plasters from the Sphinx Room (Domus Aurea, Rome). *Minerals*, Vol. 11, No. 1, pp. 1–14.
- Crupi, V., Fazio, B., Fiocco, G., Galli, G., La Russa, M. F., Licchelli, M., Majolino, D., Malagodi, M., Ricca, M., Ruffolo, S.A. and Venuti, V. (2018) Multi-analytical study of Roman frescoes from Villa dei Quintili (Rome, Italy). *Journal of Archaeological Science: Reports*, Vol. 21, pp. 422–432.
- Dayet, L. (2021) Invasive and non-invasive analyses of ochre and iron-based pigment raw materials: A methodological perspective. *Minerals*, Vol. 11, No. 2, p. 210.
- De Faria, D. L. A. and Lopes, F. N. (2007) Heated goethite and natural hematite: can Raman spectroscopy be used to differentiate them? *Vibrational Spectroscopy*, Vol. 45, No. 2, pp. 117–121.
- Delaney, J. K., Dooley, K. A., Radpour, R. and Kakoulli, I. (2017) Macroscale multimodal imaging reveals ancient painting production technology and the vogue in Greco-Roman Egypt. *Scientific Reports*, Vol. 7, No. 1, pp. 1–12.
- Di Stefano, L. M., Fuchs, R. (2011) Characterisation of the pigments in a Ptolemaic Egyptian Book of the Dead papyrus. *Archaeological and Anthropological Sciences*, Vol. 3, No. 3, pp. 229–244.
- Durán, A., Perez-Rodriguez, J. L., De Haro, M. J., Franquelo, M. L. and Robador, M. D. (2011) Analytical study of Roman and Arabic wall paintings in the Patio De Banderas of Reales Alcazares' Palace using non-destructive XRD/XRF and complementary techniques. *Journal of Archaeological Science*, Vol. 38, No. (9), pp. 2366–2377.
- Ebeling, P., Edrey, M., Harpak, T., Lichtenberger, A. and Tal, O. (2020) Field report on the 2019 German-Israeli Tell İştābbā Excavation Project (Beth She'an), Israel. *Zeitschrift des Deutschen Palästina-Vereins*, Vol. 136, No. 2, pp. 176–190.
- Ebeling, P., Edrey, M., Harpak, T., Lichtenberger, A. and Tal, O. (2021) Field report on the 2020 German-Israeli Tell İştābbā Excavation Project (Beth She'an), Israel. *Zeitschrift des Deutschen Palästina-Vereins*, Vol. 137, No. 1, pp. 60–74.
- Elias, M., Chartier, C., Prévot, G., Garay, H. and Vignaud, C. (2006) The colour of ochres explained by their composition. *Materials Science and Engineering: B*, Vol. 127, No. 1, pp. 70–80.

- Fedorov, P. P. and Samoylov A. M. (2019) Ancient Roman technology of aluminum production: Process reconstruction. *Fine Chemical Technologies*, Vol. 14, No. 6, pp. 31–38.
- Fermo, P., Piazzalunga, A., de Vos, M. and Andreoli, M. (2013) A multi-analytical approach for the study of the pigments used in the wall paintings from a building complex on the Caelian Hill (Rome). *Applied Physics A*, Vol. 113, No. 4, pp. 1109–1119.
- Finkielsztein, G. (1999) More evidence on John Hyrcanus I's conquests: Lead weights and Rhodian amphora stamps. *Bulletin of the Anglo-Israel Archaeological Society*, Vol. 16, pp. 33–63.
- Foerster, G. (1995) *Masada: The Yigael Yadin Excavations 1963–1965: Final Reports*. Art and Architecture. Jerusalem, Israel Exploration Society.
- Fostiridou, A., Karapanagiotis, I., Vivdenko, S., Lampakis, D., Mantzouris, D., Achilara, L. and Manoudis, P. (2016) Identification of pigments in Hellenistic and roman funeral figurines. *Archaeometry*, Vol. 58, No. 3, pp. 453–464.
- Gajić-Kvašček, M., Stojanović, M. M., Šmit, Ž., Kantarelou, V., Karydas, A. G., Šljivar, D., Milovanović, D. and Andrić, V. (2012) New evidence for the use of cinnabar as a colouring pigment in the Vinča culture. *Journal of Archaeological Science*, Vol. 39, No. 4, pp. 1025–1033.
- Garilli, V., Vita, G., La Parola, V., Vraca, M. P., Giarrusso, R., Rosina, P., Bonfiglio, L. and Sineo, L. (2020) First evidence of Pleistocene ochre production from bacteriogenic iron oxides. A case study of the Upper Palaeolithic site at the San Teodoro Cave (Sicily, Italy). *Journal of Archaeological Science*, Vol. 123, p. 105221.
- Gil-Torrano, A., Gómez-Morón, A., Martín, J. M., Ortiz, R., Fuertes Santos, M. and Ortiz, P. (2019) Characterization of Roman and Arabic mural paintings of the archaeological site of Cercadilla (Cordoba, Spain). *Scanning*, 1–14.
- Guirdzhiiska, D., Zlateva, B. and Glavcheva, Z. (2017) Polished decorative fields in Thracian Fresco Tombs from the Hellenistic period-Archaeometrical research. *STAR: Science & Technology of Archaeological Research*, Vol. 3, No. 2, pp. 428–436.
- Gutman, M., Zanier, K., Lux, J. and Kramar, S. (2016) Pigment analysis of Roman wall paintings from two vallae rusticae in Slovenia. *Mediterranean Archaeology & Archaeometry*, Vol. 16, No. 3, pp. 193–206.
- Holakooei, P., Karimy, A. H., Hasanpour, A. and Oudbashi, O. (2016) Micro-Raman spectroscopy in the identification of wulfenite and vanadinite in a Sasanian painted stucco fragment of the Ghaleh Guri in Ramavand, western Iran. *Spectrochimica Acta Part A: Molecular Biomolecular Spectroscopy*, Vol. 169, pp. 169–174.
- Iordanidis, A., Garcia-Guinea, J., Strati, A. and Gkimourtzina, A. (2014) A comparative study of pigments from the wall paintings of two Greek Byzantine churches. *Analytical Letters*, Vol. 47, No. 16, pp. 2708–2721.
- Kakoulli, I. (2002) Late Classical and Hellenistic painting techniques and materials: A review of the technical literature. *Studies in Conservation*, Vol. 47, No. 1, pp. 56–67.
- Kidd, B. (1999) Technique and composition of the Tel Anafa stucco. *Annual of the Museum of Art and Archaeology*, Vols. 33–35, pp. 5–13.
- Kidd, B. (2018) Decorative wall plaster. In: Berlin A. M., Herbert, S. C. (eds.), *Tel Anafa II,iii*. Ann Arbor, MI, Kelsey Museum of Archaeology, pp. 5–78.
- Klempan, B., Helwig, K. and Colivicchi, F. (2017) Examination and analysis of Etruscan wall paintings at Caere, Italy. *Archaeometry* Vol. 59, No. 6, pp. 1082–1094.
- Jackson, H. (2016) Stucco fragments from the acropolis palace. In: Clarke, G. et al. (eds.), *Jebel Khalid on the Euphrates. V. Report on Excavations 2000-2010*. *Mediterranean Archaeology Supplement* Vol. 10, Sydney, pp. 259–268.
- Jackson-Tal, R. E., Lichtenberger, A. and Tal, O. (2021) Hellenistic vitreous finds from Seleucid Tell Izṭabba (Israel). *Levant*, Vol. 52, No. 3, pp. 382–392.
- Laidlaw, A. (1985) *The First Style in Pompeii: Painting and Architecture*. Rome, Bretschneider.
- Lichtenberger, A. (2008) Artemis and Zeus Olympios in Roman Gerasa and Seleucid religious policy. In: Kaizer, T., (ed.), *The variety of local religious life in the Near East in the Hellenistic and Roman periods*. Leiden and Boston, Brill Publishers, pp. 133–153.
- Lichtenberger, A. (accessed 27 Nov 2020) Decapolis. *Brill encyclopedia of Early Christianity online*. Leiden: Brill Publishers. https://doi.org/10.1163/2589-7993_EECO_SIM_00000878.
- Lichtenberger, A., Meyer, C. and Tal, O. (2020) Magnetic prospecting at Nysa-Scythopolis (Tell Izṭabba, Beth She'an, Israel): Deciphering urban planning at a newly founded Hellenistic town of the Decapolis. *STRATA: Bulletin of the Anglo-Israel Archaeological Society*, Vol. 38, pp. 45–70.
- Ling, R. (1991) *Roman Painting*. Cambridge, Cambridge University Press, pp. 12–99.

- Linn, R. (2017) Layered pigments and painting technology of the Roman wall paintings of Caesarea Maritima. *Journal of Archaeological Science: Reports*, Vol. 11, pp. 774–781.
- Liritzis, I., Laskaris, N., Vafiadou, A., Karapanagiotis, I., Volonakis, P., Papageorgopoulou, C. and Bratitsi, M. (2020) Archaeometry: an overview. *Scientific Culture*, Vol. 6, No. 1, pp. 49–98. DOI: 10.5281/zenodo.3625220
- Maeir A. M. (2020) Chapter 1: The Beth-Shean Valley: Geographical and environmental background. In: Mazar A. and Panitz-Cohen N., (eds.), *Tel Rehov: A Bronze and Iron Age City in the Beth-Shean Valley, Volume I: Introductions, Synthesis and Excavations on the Upper Mound. Qedem 59*. Jerusalem, Hebrew University of Jerusalem, pp. 1–11.
- Marcaida, I., Maguregui, M., Fdez-Ortiz de Vallejuelo, S., Morillas, H., Prieto-Taboada, N., Veneranda, M., Castro, K. and Madariaga, J. M. (2017) In situ X-ray fluorescence-based method to differentiate among red ochre pigments and yellow ochre pigments thermally transformed to red pigments of wall paintings from Pompeii. *Analytical and Bioanalytical Chemistry*, Vol. 409, No. 15, pp. 3853–3860.
- Marcaida, I., Maguregui, M., Morillas, H., Prieto-Taboada, N., de Vallejuelo, S. F. O., Veneranda, M., Madariaga, J. M., Martellone, A., De Nigris, B. and Osanna, M. (2018). In situ non-invasive characterization of the composition of Pompeian pigments preserved in their original bowls. *Microchemical Journal*, Vol. 139, pp. 458–466.
- Marketou, A. K., Kouzeli, K. and Facorellis, Y. (2019) Colourful earth: Iron-containing pigments from the Hellenistic pigment production site of the ancient agora of Kos (Greece). *Journal of Archaeological Science: Reports*, Vol. 26, 101843.
- Mateos, L. D., Cosano, D., Mora, M., Muniz, I., Carmona, R., Jimenez-Sanchidrian, C. and Ruiz, J. R. (2015) Raman microspectroscopic analysis of decorative pigments from the Roman villa of El Ruedo (Almedinilla, Spain). *Spectrochimica Acta Part A: Molecular and Biomolecular Spectroscopy*, Vol. 151, pp. 16–21.
- Mateos, L. D., Esquivel, D., Cosano, D., Jiménez-Sanchidrián, C. and Ruiz, J. R. (2018). Micro-Raman analysis of mortars and wallpaintings in the Roman villa of Fuente Alamo (Puente Genil, Spain) and identification of the application technique. *Sensors and Actuators A: Physical*, Vol. 281, pp. 15–23.
- Mazor, G., Atrash, W. and Finkielsztein, G. (2018) Bet She'an IV. Hellenistic Nysa-Scythopolis: The amphora stamps and sealings from Tel Iztabba. *Israel Antiquities Authority Report*, p. 62.
- Mazzocchin, G. A., Agnoli, F., Mazzocchin, S. and Colpo, I. (2003) Analysis of pigments from Roman wall paintings found in Vicenza. *Talanta*, Vol. 61, No. 4, pp. 565–572.
- Miriello, D., Bloise, A., Crisci, G. M., De Luca, R., De Nigris, B., Martellone, A., Osanna, M., Pace, R., Pecci, A. and Ruggieri, N. (2018). Non-destructive multi-analytical approach to study the pigments of wall painting fragments reused in mortars from the archaeological site of Pompeii (Italy). *Minerals*, Vol. 8, No. 4, p. 134.
- Miriello, D., De Luca, R., Bloise, A., Niceforo, G. and Daniel, J. (2021). Pigments mapping on two mural paintings of the “house of garden” in Pompeii (Campania, Italy). *Mediterranean Archaeology and Archaeometry*, Vol. 21, No. 1, pp. 257–271. DOI: 10.5281/zenodo.4574643.
- Mortimore, J. L., Marshall, L. J. R., Almond, M. J., Hollins, P. and Matthews, W. (2004) Analysis of red and yellow ochre samples from Clearwell Caves and Çatalhöyük by vibrational spectroscopy and other techniques. *Spectrochimica Acta Part A: Molecular and Biomolecular Spectroscopy*, Vol. 60, No. 5, pp. 1179–1188.
- Olivares, M., Castro, K., Corchón, M. S., Gárate, D., Murelaga, X., Sarmiento, A. and Etxebarria, N. (2013) Non-invasive portable instrumentation to study Palaeolithic rock paintings: the case of La Peña Cave in San Roman de Candamo (Asturias, Spain). *Journal of Archaeological Science*, Vol. 40, No. 2, pp. 1354–1360.
- Orendi, A., Lichtenberger, A. and Tal, O. (2021) Food in a colonial setting: The flora assemblage of a short-lived Seleucid-founded site in the Near East. *Vegetation History and Archaeobotany*, Vol. 30. <https://doi.org/10.1007/s00334-020-00820-z>.
- Piovesan, R., Maritan, L., Amatucci, M., Nodari, L. and Neguer, J. (2016). Wall painting pigments of Roman Empire age from Syria Palestina province (Israel). *European Journal of Mineralogy*, Vol. 28, No. 2, pp. 435–448.
- Radpour, R., Fischer, C. and Kakoulli, I. (2019) New insight into Hellenistic and Roman Cypriot wall paintings: an exploration of artists' materials, production technology, and technical style. *Arts*, Vol. 8, No. 2, p. 74.

- Rao, D. S., Vijayakumar, T. V., Prabhakar, S. and Raju, G. B. (2011) Geochemical assessment of a siliceous limestone sample for cement making. *Chinese Journal of geochemistry*, Vol. 30, No. 1, pp. 33–39.
- Roebroeks, W., Sier, M. J., Nielsen, T. K., De Loecker, D., Parés, J. M., Arps, C. E. and Múcher, H. J. (2012). Use of red ochre by early Neandertals. *Proceedings of the National Academy of Sciences*, Vol. 109, No. 6, 1889–1894.
- Román, R. S., Bañón, C. B. and Ruiz, M. D. L. (2015) Analysis of the red ochre of the El Mirón burial (Ramales de la Victoria, Cantabria, Spain). *Journal of Archaeological Science*, Vol. 60, pp. 84–98.
- Rozenberg, S. (2008) Hasmonean and Herodian Palaces at Jericho. Final Reports of the 1973–1987 Excavations. *Volume IV: The Decoration of Herod's Third Palace at Jericho*. Jerusalem, Israel Exploration Society and The Hebrew University of Jerusalem.
- Rozenberg, S. (2014) Wall painters in Herodian Judea. Wall Painters in Herodian Judea. *Near Eastern Archaeology*, Vol. 77, No. 2, pp. 120–128.
- Sabbatini, L., Tarantino, M. G., Zambonin, P. G. and De Benedetto, G. E. (2000) Analytical characterization of paintings on pre-Roman pottery by means of spectroscopic techniques. Part II: Red, brown and black colored shards. *Fresenius' Journal of Analytical Chemistry*, Vol. 366, No. 1, pp. 116–124.
- Siddall, R. (2018) Mineral pigments in archaeology: their analysis and the range of available materials. *Minerals*, Vol. 8, No. 5, p. 201.
- Segal, I. and Porat, N. (1997) Composition of pigments from the Hellenistic walls in Acre. In: Bearat H, Fuchs M, Maggetti M, Paunier D. (eds.), *Roman Wall Painting: Materials, Techniques, Analysis and Conservation*. Fribourg: Proceed Inter Workshop, pp. 85–92.
- Siddall, R. (2018) Mineral pigments in archaeology: their analysis and the range of available materials. *Minerals*, Vol. 8, No. 5, p. 201.
- Szczepaniak, M. (2014) Rock materials in monuments and archaeology—research methods. In: Michalska, D. and Szczepaniak, M. (Eds.), *Geoscience in Archaeometry. Methods and Case Studies*. Poznań, Bogucki Wydawnictwo Naukowe Publisher, pp. 13–36.
- Taglieri, G., Rigaglia, D., Arrizza, L., Daniele, V., Macera, L., Rosatelli, G., Romè, V. and Musolino, G. (2019) Microanalytical investigations on a Byzantine fresco of the Dormitio Virginis from Sicily. *Journal of Cultural Heritage*, Vol. 40, pp. 155–162.
- Tal, O. (2011) 'Hellenistic foundations' in Palestine. In: Grabbe L. I. and Lipschits O. (Eds.), *Judah between East and West: The Transition from Persian to Greek Rule (ca. 400–200 BCE)*, New York/London, *Library of Second Temple Studies* Vol. 74, pp. 242–254.
- Tal, O. and Reshef, N. (2017) Hellenistic stratigraphy and architecture. In: Greenberg, R., Tal, O., Da'adli, T. Bet Yerah, *Vol. III: Hellenistic Philoteria and Islamic al-Şinnabra*. Jerusalem: IAA Reports Vol. 61, pp. 13–58.
- Tomasini, E., Siracusano, G. and Maier, M. S. (2012) Spectroscopic, morphological and chemical characterization of historic pigments based on carbon. Paths for the identification of an artistic pigment. *Microchemical Journal*, Vol. 102, 28–37.
- Tsatskin, A. and Gendler, T. S. (2016) Identification of "red ochre" in soil at Kfar HaHoresh Neolithic site, Israel: Magnetic measurements coupled with materials characterization. *Journal of Archaeological Science: Reports*, Vol. 6, pp. 284–292.
- Vázquez de Ágredos-Pascual, M. L., Zapata-Meza, M., Sanz-Rincón, R., Garza DíazBarriga, A., Expósito De Vicente, C., Rojo-Iranzo, L., Herreras Sala, S. (2019) Physicochemical and cultural study of coloring materials from 1st c. AD Magdala, Lower Galilee. *Mediterranean Archaeology and Archaeometry*, Vol. 19, No. 3, pp. 173–188. DOI: 10.5281/zenodo.3583077.
- Wadley, L. (2009) Post-depositional heating may cause over-representation of red-coloured ochre in Stone Age sites. *South African Archaeological Bulletin*, Vol. 64, No. 190, pp. 166–171.
- Westlake, P., Siozos, P., Philippidis, A., Apostolaki, C., Derham, B., Terlix, A., Perdikatsis, V., Jones, R. and Anglos, D. (2012) Studying pigments on painted plaster in Minoan, Roman and Early Byzantine Crete. A multi-analytical technique approach. *Analytical and bioanalytical chemistry*, Vol. 402, No. 4, pp. 1413–1432.
- Winter, J. (1983) The characterization of pigments based on carbon. *Studies in Conservation*, Vol. 28, No. 2, pp. 49–66.